A Class of Linear–Nonlinear Switching Active Disturbance Rejection Speed and Current Controllers for PMSM

Ping Lin, Zhen Wu, Kun-Zhi Liu, and Xi-Ming Sun, *Senior Member, IEEE*

***Abstract*—This article investigates a class of linear–nonlinear switching active disturbance rejection control (ADRC) to design speed controllers and current controllers for permanent magnet synchronous machine (PMSM) in servo systems, which aims at enhancing the ability of disturbance rejection of speed and current controllers for PMSM. First, the mathematical model of PMSM is introduced. Next, the design of a class of linear–nonlinear switching ADRCs is introduced in details. Then, the stability of linear–nonlinear switching extended state observers (ESOs) is proved by multiple Lyapunov functions. Lastly, the effectiveness of the speed and current controllers based on the linear–nonlinear active disturbance rejection technique is validated by experiments results of a 5.5-kW PMSM platform. Specially, the experiment results of the speed controllers illustrate that the amplitude of speed change of the proposed ADRCs is smaller than that of the linear ADRC (LADRC) when the step load torque disturbance occurs. The proposed ADRCs can overcome the overshoot of speed response caused by improper parameter setting of LADRC. The experiment results of the current controllers show that the proposed LNSADRC type 2 has greater robustness than the other ADRC controllers when b_{02} is not estimated accurately.**

***Index Terms*—Current controller, extended state observer (ESO), linear–nonlinear switching active disturbance rejection control (ADRC), permanent magnet synchronous motor (PMSM), speed controller.**

I. Introduction

IT IS WELL known that servo systems adopt electrical machines to realize the tracking of speed and position signals, such as computerized numerical control machine tool [1] and multi-axis servo systems [2]. Especially in aviation application, servo systems are prevalent in more electric aircraft (MEA), such as A380 and B787, which can contribute to the reduction of consumption of nonpropulsive power and then reduce total fuel consumption [3]. MEA can also reduce maintenance costs while increase the operational reliability [4]. To be more specific, servo systems, such as electrical starter/generator and electromechanical actuators, are one of the most important parts of the MEA. Increasing the robustness of the above systems is of great significance. On the one hand, some starter/generators with new structure have been designed to enhance the reliability, such as a doubly salient starter/generator with two-section twisted-rotor structure in [5] and doubly salient permanent magnet machine in [6]. On the other hand, improving the robustness of the control system should be paid more attention without changing the hardware structure.

Generally speaking, cascade control structure can be adopted to enhance the robustness of the control system, which includes the outer speed loop controller and the inner current loop controller. A large number of control algorithms with the aim of realizing disturbance attenuation have been proposed to design the speed controller and the current controller, such as proportional-integral (PI) control with feed-forward compensation, disturbance-based control [7], slide mode control (SMC), active disturbance rejection control (ADRC), and so on. In order to enhance the robustness of speed controller, many advanced algorithms are proposed (see [8]–[21]). We just list some of them. A new sliding-mode reaching law was proposed in [8] to overcome the chattering of SMC, which includes the system state variable and the power term of sliding surface function. The key point is that the power term is bounded by the absolute value of the switching function, which can attenuate the inherent chattering and speed up the convergence of the system state to the sliding mode surface. Specially, a revised extended state observer (ESO) is designed to calculate the total disturbance [8] which has enhanced the disturbance attenuation ability of the plant. A similar sophisticated framework is also introduced in [9]. A novel adaptive terminal sliding mode reaching law is proposed in [9] which has better tracking performance and more alleviating chattering compared with those traditional sliding mode reaching law by experiments. Furthermore, the total disturbances are estimated by the extended sliding mode observer, which strengthens the disturbance rejection ability of the plant [9]. The corresponding research in current controller has aroused the

Manuscript received January 3, 2021; revised April 17, 2021; accepted May 28, 2021. Date of publication June 3, 2021; date of current version August 16, 2021. This work was supported in part by the National Natural Science Foundation of China under Grants 61890920 and 61890921, in part by LiaoNing Revitalization Talents Program under Grant XLYC1808015, in part by National Science and Technology Major Project under Grants J2019-V-0010-0105 and 2017-V-0005-0055, and in part by the Fundamental Research Funds for the Central Universities of China with Grant Nos. DUT21RC(3)040. Recommended for publication by Associate Editor K. Akatsu. *(Corresponding author: Xi-Ming Sun.)*

Ping Lin, Kun-Zhi Liu, and Xi-Ming Sun are with the Key Laboratory of Intelligent Control and Optimization for Industrial Equipment of Ministry of Education, Dalian University of Technology, Dalian 116024, China, and also with the School of Control Science and Engineering, Dalian University of Technology, Dalian 116024, China (e-mail: dmulinping@mail.dlut.edu.cn; kzliu1989@dlut.edu.cn; sunxm@dlut.edu.cn).

Zhen Wu is with the School of Aeronautics and Astronautics, Dalian University of Technology, Dalian 116024, China (e-mail: wzxx@mail.dlut.edu.cn).

Color versions of one or more figures in this article are available at https://doi.org/10.1109/TPEL.2021.3086273.

Digital Object Identifier 10.1109/TPEL.2021.3086273

enthusiasm of many scientific and technical researchers, such as predictive current control [22]–[26] and SMC [22].

The ADRC is also a good candidate to attenuate disturbance, and the corresponding academic research has been done by scientific researchers (see [27]–[35]). For example, the gain of ESO is subjected to sensor sampling frequency, which means that the gain of ESO is limited. The nonlinear ADRC may have smaller gain of ESO compared with that of linear ADRC while can possess the same accuracy of total disturbance estimation [33]. However, the magnitude or gradient of the total disturbance affects the prediction accuracy of ESO. To be more accurate, the performance of the nonlinear ADRC may begin to degenerate when the magnitude or gradient of the total disturbance becomes large to a certain degree [34]. While the deterioration of linear ADRC performance will not sharply take place when the magnitude or rate of changing of the total disturbance turns big [34]. Toward that end, integrating the merits of linear ADRC and nonlinear ADRC together is of great usefulness. How to integrate the strengths of linear ADRC and nonlinear ADRC together should be investigated in depth. Switching is an effective method to integrate linear ADRC and nonlinear ADRC seamlessly together. Thus, the linear–nonlinear switching ADRC has attracted the attention of some scholars recently. For example, a linear–nonlinear switching ADRC is proposed to estimate the total disturbances, which has been verified in ball-beam system [34] and the PMSM system [30]. The experiment results of ball-beam system illustrate that the linear–nonlinear switching ADRC possesses the merits of linear ADRC and nonlinear ADRC [34], which is sophisticated and pioneered.

However, as for the linear–nonlinear switching ADRC, stability analysis is of great challenge compared with the linear ADRC. To be more specific, the traditional methods for linear systems are not suitable for nonlinear systems. Lyapunov function is an effective tool to analyze the stability of the nonlinear systems. Nevertheless, constructing Lyapunov function is challenging. There is less literature illustrating how to prove the stability of linear–nonlinear switching ADRC by Lyapunov functions compared with the linear ADRC. Especially, how to construct Lyapunov function of linear–nonlinear switching ADRC designed by different switching rules is of great skill.

Based on the above observation, inspired by [8], [9], [30], [34], a novel class of linear–nonlinear switching ADRCs are proposed to design the speed controller and current controller for PMSM, whose goal is to strengthen the robustness of the control systems of the PMSM. Furthermore, the proposed ADRCs integrate the traditional ESO and linear ESO together seamlessly by observation error. Such work may be of great significance, which can be extended in other engineering scenarios.

The contribution of this article is to design the speed controller and current controller in PMSM by using linear–nonlinear switching ADRC. Multiple Lyapunov functions are constructed to prove the stability of linear–nonlinear switching ESOs. Finally, the effectiveness of the speed and current controllers based on the linear–nonlinear active disturbance rejection technique is validated by experiments results of a 5.5-kW PMSM platform.

The rest of the article is presented as follows. The problem is formulated in Section II. Section III presents the linear–nonlinear switching ADRCs for speed controller for PMSM. Section IV illustrates the linear–nonlinear switching ADRCs for current controller for PMSM. The relationship between ADRC and PI is revealed in Section V. Next, multiple Lyapunov functions are constructed to prove the stability of linear–nonlinear switching ESO and the transfer function method is used to analyze the stability of the closed-loop system, which is illustrated in Section VI. And the detailed deduction is presented in the Appendix A and Appendix B. Furthermore, experiment results and the corresponding discussions are given in Section VII. Lastly, we conclude the whole article in Section VIII.

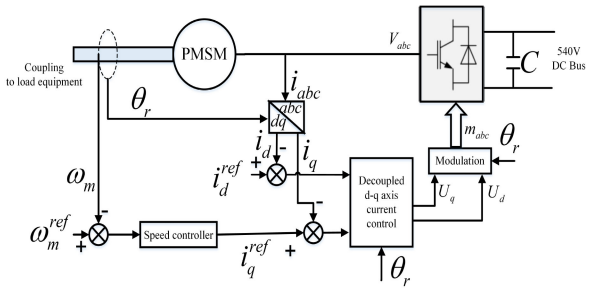

Fig. 1. Control system of the PMSM coupling to load equipment.

II. Problem Formulation

According to the common sense in [36], the mathematical model of PMSM in the d–q axis of the rotor synchronous rotation coordinate system can be obtained.

The stator voltage equations are given as follows:

$$U_d = R_s i_d + \frac{d\Psi_d}{dt} - \omega_r \Psi_q \tag{1}$$

$$U_q = R_s i_q + \frac{d\Psi_q}{dt} + \omega_r \Psi_d. \tag{2}$$

The stator flux equations are shown as follows:

$$\Psi_d = L_d i_d + \Psi_f \tag{3}$$

$$\Psi_q = L_q i_q. \tag{4}$$

The electromagnetic torque equation is presented as follows:

$$T_e = \frac{3}{2} n_p (\Psi_d i_q - \Psi_q i_d). \tag{5}$$

The motion equation is illustrated as follows:

$$T_e - T_L - B\omega_m = \frac{J}{n_p} \frac{d\omega_r}{dt} \tag{6}$$

where U_d, U_q, i_d, i_q, L_q, L_d, and Ψ_d, Ψ_q in (1)–(6) are, respectively, the voltage, the current, the inductance, and the flux linkage in the d–q axis of the rotor synchronous rotation coordinate system. R_s is the stator winding phase resistance. ω_r is the electrical angular velocity of the PMSM rotor. ω_m is the mechanical angular velocity of the PMSM. Ψ_f is the flux amplitude of permanent magnet. n_p is the pole pairs of PMSM. $\omega_m n_p = \omega_r$. T_e is the electromagnetic torque of PMSM. T_L is

the load torque from load equipment in Fig. 1. *J* is the moment of inertia of PMSM. B is the viscous frictional coefficient.

In Fig. 1, load equipment may be gas turbine, oil pump, etc. On the one hand, how to devise a speed controller to enhance the robustness of the control system should be investigated. In the next section, a speed controller in possession of disturbance rejection ability is proposed. To improve the disturbance rejection ability, the speed controller in Fig. 1 is replaced by the proposed linear–nonlinear switching ADRCs, which is shown in Section III. Furthermore, the current controllers will also be devised by the proposed linear–nonlinear switching ADRCs, which is introduced in Section IV.

III. Design of Linear–Nonlinear Switching Active Disturbance Rejection Speed Controllers

In general, it is prevalent that cascade control structure consists of the speed controller and the current controller [37]. In order to enhance the robustness of the controller of the speed loop, a speed controller based on linear–nonlinear switching ADRC is introduced in details. The controller of the current loop adopts PI algorithm. Note that the bandwidth of current loop is faster than that of the bandwidth of speed loop. Thus, i_q^{ref} is equal to i_q when the speed loop is in transient process, where i_q^{ref} is the reference value of i_q. This assumption is introduced in [38].

By the simple deduction from the equalities (1)–(6), the following mathematical expressions can be got:

$$\dot{\omega}_m = \frac{3n_p\Psi_d}{2J} i_q + f_m \tag{7}$$

$$\dot{i}_q = \frac{U_q}{L_q} + f_q \tag{8}$$

$$\dot{i}_d = \frac{U_d}{L_d} + f_d \tag{9}$$

where

$$f_m = -\frac{T_L}{J} - \frac{B\omega_m}{J}$$

$$f_q = -\frac{R_s i_q}{L_q} - \frac{\omega_r L_d i_d + \omega_r \Psi_f}{L_q}$$

$$f_d = -\frac{R_s i_d}{L_d} + \frac{\omega_r L_q i_q}{L_d}.$$

Equations (7)–(9) are the canonical forms for designing ADRC. We give an example how to design ADRC in speed loop. Equation (7) can be recast as

$$\begin{cases} \dot{x}_1 = b_0 \cdot i_q + x_2 \\ \dot{x}_2 = -h \end{cases} \tag{10}$$

where $x_1 = \omega_m$, $b_m = \frac{3n_p\Psi_d}{2J}$, $x_2 = f_m + (b_m - b_0)i_q$ and b_0 is the estimated value of b_m.

A class of linear–nonlinear switching ADRCs are given in the next subsection by adopting different linear–nonlinear switching ESOs. To avoid confusion, the corresponding controllers are named as linear–nonlinear switching ADRC type 1 (LNSADRC type 1) and linear–nonlinear switching ADRC type 2 (LNSADRC type 2), respectively. In comparison with linear ESOs, linear–nonlinear switching ESOs integrate the merits of linear ESOs and nonlinear ESOs together and eliminate the demerits of traditional ESOs [34].

A. Linear–Nonlinear Switching ADRC Type 1

Define $\upsilon_1 = \omega_m^{ref}$ and $e_1 = z_1 - \omega_m$. e_1 is the observation error. Inspired by [34], the first linear–nonlinear switching ESO for (10) is presented as follows:

$$\begin{cases} \dot{z}_1 = z_2 - \beta_{11}e_1 + b_0 \cdot i_q \\ \dot{z}_2 = -F_2 \cdot fal(e_1, \alpha_2, \delta_1, \delta_2) \end{cases} \tag{11}$$

where z_n are estimated values of x_n with $n \in \{1, 2\}$. The mathematical expression of $F_2 \cdot fal(e_1, \alpha_2, \delta_1, \delta_2)$ can be described as follows:

$$F_2 \cdot fal(e_1, \alpha_2, \delta_1, \delta_2) = \begin{cases} \beta_{21}^{(3)} \dfrac{e_1}{\delta_1^{1-\alpha_2}}, |e_1| \le \delta_1 \\ \beta_{21}^{(2)} |e_1|^{\alpha_2} sign(e_1) \\ \delta_1 < |e_1| \le \delta_2 \\ \beta_{21}^{(1)} e_1, |e_1| > \delta_2. \end{cases} \tag{12}$$

Equation (12) adopts discontinuous switching, which is different from the method introduced in [34]. β_{11}, $\beta_{21}^{(1)}$, $\beta_{21}^{(2)}$, and $\beta_{21}^{(3)}$ are gain coefficients of ESO. The control law is $i_q^{ref} = \frac{u_0 - z_2}{b_0}$ and $u_0 = k_{11}(\upsilon_1 - z_1)$, where b_0 is the estimated value of b_m and k_{11} is the control gain.

Define $e_2 = z_2 - x_2$. The error state equations from (10) and (11) are shown as follows:

$$\begin{cases} \dot{e}_1 = e_2 - \beta_{11}e_1 \\ \dot{e}_2 = h - F_2 \cdot fal(e_1, \alpha_2, \delta_1, \delta_2). \end{cases} \tag{13}$$

The stability of (13) is proved in Appendix A.

B. Linear–Nonlinear Switching ADRC Type 2

Define $\upsilon_1 = \omega_m^{ref}$ and $e_1 = z_1 - \omega_m$. The corresponding linear–nonlinear switching ESO for (10) is presented as follows:

$$\begin{cases} \dot{z}_1 = z_2 - F_1 \cdot fal(e_1, \alpha_1, \delta_1, \delta_2) + b_0 \cdot i_q \\ \dot{z}_2 = -F_2 \cdot fal(e_1, \alpha_2, \delta_1, \delta_2) \end{cases} \tag{14}$$

where z_n are estimated values of x_n with $n \in \{1, 2\}$. $\beta_{i1}^{(1)}$, $\beta_{i1}^{(2)}$ and $\beta_{i1}^{(3)}$ are gain coefficients of ESO. The control law is illustrated as $i_q = \frac{u_0 - z_2}{b_0}$ and $u_0 = k_{11}(\upsilon_1 - z_1)$. The mathematical expression of $F_i \cdot fal(e_1, \alpha_i, \delta_1, \delta_2)$ is illustrated as follows:

$$F_i \cdot fal(e_1, \alpha_i, \delta_1, \delta_2) = \begin{cases} \beta_{i1}^{(3)} \dfrac{e_1}{\delta_1^{1-\alpha_i}}, |e_1| \le \delta_1 \\ \beta_{i1}^{(2)} |e_1|^{\alpha_i} sign(e_1) \\ \delta_1 < |e_1| \le \delta_2 \\ \beta_{i1}^{(1)} e_1, |e_1| > \delta_2 \end{cases} \tag{15}$$

where $i \in \{1, 2\}$.

Define $e_2 = z_2 - x_2$. The error state equations from (10) and (14) are shown as follows:

$$\begin{cases} \dot{e}_1 = e_2 - F_1 \cdot fal(e_1, \alpha_1, \delta_1, \delta_2) \\ \dot{e}_2 = h - F_2 \cdot fal(e_1, \alpha_2, \delta_1, \delta_2). \end{cases} \tag{16}$$

The stability of (16) is presented in Appendix B.

C. Linear–Nonlinear Switching ADRC Type 3

This subsection introduces the linear–nonlinear switching ADRC presented in [34], which is called linear–nonlinear switching ADRC type 3 (LNSADRC type 3). Define $\upsilon_1 = \omega_m^{ref}$ and $e_1 = z_1 - \omega_m$. The corresponding linear–nonlinear switching ESO for (10) is presented as follows:

$$\begin{cases} \dot{z}_1 = z_2 - \beta_{11} e_1 + b_0 \cdot i_q \\ \dot{z}_2 = -\beta_{21} \cdot fal(e_1, \alpha_2, \delta_1, \delta_2) \end{cases} \tag{17}$$

where z_n are estimated values of x_n with $n \in \{1, 2\}$. β_{21} and β_{11} are gain coefficients of ESO. The control law is illustrated as $i_q = \frac{u_0 - z_2}{b_0}$ and $u_0 = k_{11}(\upsilon_1 - z_1)$. The mathematical expression of $fal(e_1, \alpha_2, \delta_1, \delta_2)$ can be shown as follows:

$$fal(e_1, \alpha_2, \delta_1, \delta_2) = \begin{cases} \dfrac{e_1}{\delta_1^{1-\alpha_2}}, |e_1| \le \delta_1 \\ |e_1|^{\alpha_2} sign(e_1) \\ \delta_1 < |e_1| \le \delta_2 \\ e_1, |e_1| > \delta_2. \end{cases} \tag{18}$$

Define $e_2 = z_2 - x_2$. The error state equations from (10) and (17) are shown as follows:

$$\begin{cases} \dot{e}_1 = e_2 - \beta_{11} e_1 \\ \dot{e}_2 = h - \beta_{21} \cdot fal(e_1, \alpha_2, \delta_1, \delta_2). \end{cases} \tag{19}$$

The stability of (19) is proved by Li [34], which is introduced in Section I.

D. Linear ADRC

This section introduces the linear ADRC, which is called LADRC. Define $\upsilon_1 = \omega_m^{ref}$ and $e_1 = z_1 - \omega_m$. The corresponding ESO for (10) is presented as follows:

$$\begin{cases} \dot{z}_1 = z_2 - \beta_{11} e_1 + b_0 \cdot i_q \\ \dot{z}_2 = -\beta_{21} e_1 \end{cases} \tag{20}$$

where z_n are estimated values of x_n with $n \in \{1, 2\}$. The control law is illustrated as $i_q = \frac{u_0 - z_2}{b_0}$ and $u_0 = k_{11}(\upsilon_1 - z_1)$. Define $e_2 = z_2 - x_2$. The error state equations from (10) and (20) are illustrated as follows:

$$\begin{cases} \dot{e}_1 = e_2 - \beta_{11} e_1 \\ \dot{e}_2 = h - \beta_{21} e_1. \end{cases} \tag{21}$$

The stability of (21) is analyzed in [39].

IV. Design of Linear–Nonlinear Switching Active Disturbance Rejection Current Controllers

The current loop controllers can be designed by using the linear–nonlinear switching ADRC type 1, the linear–nonlinear switching ADRC type 2, the linear–nonlinear switching ADRC type 3, and the linear ADRC. The detailed process is similar to the speed loop controllers designed by the above ADRCs. In order to save limited space, we omit it here. The speed controller parameter symbols α_1, α_2, δ_1, δ_2, β_{11}, β_{21}, $\beta_{11}^{(1)}$, $\beta_{11}^{(2)}$, $\beta_{11}^{(3)}$, $\beta_{21}^{(1)}$, $\beta_{21}^{(2)}$, $\beta_{21}^{(3)}$, b_0, and k_{11} are replaced by α_{12}, α_{22}, δ_{12}, δ_{22}, β_{12}, β_{22}, $\beta_{12}^{(1)}$, $\beta_{12}^{(2)}$, $\beta_{12}^{(3)}$, $\beta_{22}^{(1)}$, $\beta_{22}^{(2)}$, $\beta_{22}^{(3)}$, b_{02}, and k_{12} for current controller parameter symbols, respectively, where b_{02} is the estimated value of b_q with $b_q = \frac{1}{L_q}$.

V. Stability and Convergence of the Proposed ADRCs

First, the convergence of linear–nonlinear switching ESOs with different rules is given. Second, the stability of the closed-loop system is proved by transfer functions.

A. Stability of Linear–Nonlinear Switching ESO in LNSADRC Type 1

We present a theorem to show that the linear–nonlinear switching ESO in LNSADRC type 1 is bounded-input-bounded-output (BIBO) stability.

Theorem 1: If the parameters of system (13) satisfy $0 < \alpha_2 = \frac{n}{m} < 1$, $\beta_{11} > 0$, $\beta_{21}^{(1)} > 0$, $\beta_{21}^{(2)} > 0$, $\beta_{21}^{(3)} > 0$, $3n > m$, $2m\beta_{21}^{(2)} = (m+n)\beta_{21}^{(3)}$, $n > 0$, $|\delta_2|^{\frac{n}{m}-1} = \frac{\beta_{21}^{(1)}}{\beta_{21}^{(3)}}$, and $|h| \le R_1$, where R_1 is positive number, then for any compact set $\mathcal{Q}$, there exists a constant $N > 0$ such that any solution e of the system (13) with initial value $e(0) \in \mathcal{Q}$ satisfies $\|e(t)\| \le N$ for all $t \ge 0$.

The proof of Theorem 1 is presented in Appendix VIII.

B. Stability of Nonlinear–Linear Switching ESO in LNSADRC Type 2

The following theorem shows that the linear–nonlinear switching ESO in LNSADRC type 2 is BIBO stability.

Theorem 2: If the parameters of system (16) satisfy $0 < \alpha_2 = \frac{n}{m} < \alpha_1 = \frac{q}{p} < 1$, $\beta_{i1}^{(1)} > 0$, $\beta_{i1}^{(2)} > 0$, $\beta_{i1}^{(3)} > 0$, $2m\beta_{21}^{(2)} = (m+n)\beta_{21}^{(3)}$, $3n > m$, $1 < \frac{2n}{m} + \frac{q}{p}$, $|\delta_2|^{\frac{n}{m}-1} = \frac{\beta_{21}^{(1)}}{\beta_{21}^{(3)}}$ and $|h| \le R_1$, where R_1 is positive number, then for any compact set $\mathcal{O}$, there exists a constant $M > 0$ such that any solution e of the system (16) with initial value $e(0) \in \mathcal{O}$ satisfies $\|e(t)\| \le M$ for all $t \ge 0$.

The proof of Theorem 2 is given in Appendix IX.

C. Stability of the Closed-Loop System

Theorem 3: Consider the closed-loop system (i) constituting of (10)–(12) with the control law $i_q = \frac{k_{11}(\upsilon_1 - z_1) - z_2}{b_0}$ satisfying $k_{11} > 0$. If the conditions of Theorem 1 hold, then the closed-loop system (i) is stable.

Theorem 4: Consider the closed-loop system (ii) constituting of (10), (14), and (15) with the control law $i_q = \frac{k_{11}(v_1 - z_1) - z_2}{b_0}$ satisfying $k_{11} > 0$. If the conditions of Theorem 2 hold, then the closed-loop system (ii) is stable.

Proof: Substituting (11) and $i_q = \frac{k_{11}(v_1 - z_1) - z_2}{b_0}$ into (10), we can obtain

$$\dot{x}_1 = k_{11}(\omega_m^{ref} - z_1 - x_1 + x_1) - z_2 + x_2. \tag{22}$$

Equation (22) can be recast as

$$\dot{x}_1 = k_{11}(\omega_m^{ref} - x_1 - e_1) - e_2. \tag{23}$$

Theorem 1 can guarantee that e_1 and e_2 are bounded. By Laplace transformation, three transfer functions can be obtained

$$\frac{\Omega_m(s)}{\Omega_m^{ref}(s)} = \frac{k_{11}}{s + k_{11}} \tag{24}$$

$$\frac{X_1(s)}{E_1(s)} = -\frac{k_{11}}{s + k_{11}} \tag{25}$$

$$\frac{X_1(s)}{E_2(s)} = -\frac{1}{s + k_{11}} \tag{26}$$

where $\Omega_m^{ref}(s)$, $\Omega_m(s)$, $E_1(s)$, and $E_2(s)$ are Laplace transformation of ω_m^{ref}, ω_m, e_1, and e_2, respectively. The poles of the transfer functions (24)–(26) locate in the left plane of the complex frequency domain. Thus, we can conclude that the closed-loop system (i) constituting of (10)–(12) with the control law $i_q = \frac{k_{11}(v_1 - z_1) - z_2}{b_0}$ is stable. The proof of Theorem 3 is finished.

The proof of Theorem 4 is similar to the proof of Theorem 3, so we omit it here.

VI. Relationship Between ADRC and PI

How to compare the controller performance of the proposed ADRC with that of the LADRC and the PI should be discussed in details. A rigorous justification is pursued by academic researchers. Thus, we try our best to establish the corresponding criterion to satisfy such requirements.

First, the relationship between the linear ADRC and the PI is revealed [40], [41]. To be more accurate, it proves that the first-order LADRC is equivalent to a PI controller with a low-pass filter [40]. And it reveals that the second-order LADRC can be interpreted as a PID controller with a low-pass filter [41]. They reveal that the LADRC can have better ability to attenuate overshoot and measurement noise [40], [41]. In this article, we cite the corresponding results, which are shown in Fig. 2. δ_n stands for measurement noise and δ_w is input disturbance. r is the reference value. y is the controlled output. u is the control input. The $C(s)$ and $H(s)$ in Fig. 2 can be illustrated as follows:

$$H(s) = \frac{(s^2 + \beta_{11}s + \beta_{21})k_{11}}{(\beta_{11}k_{11} + \beta_{11})s + \beta_{21}k_{11}} \tag{27}$$

$$C(s) = \frac{(\beta_{11}k_{11} + \beta_{11})s + \beta_{21}k_{11}}{b_m s(s + \beta_{11} + k_{11})}. \tag{28}$$

$C(s)$ can be recast as

$$C(s) = C_{PI}(s)F_{L1}(s) \tag{29}$$

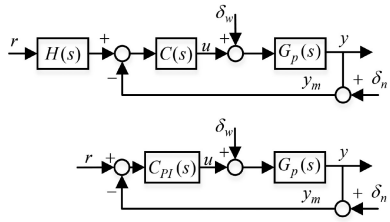

Fig. 2. Relationship of PI and the first-order LADRC [42].

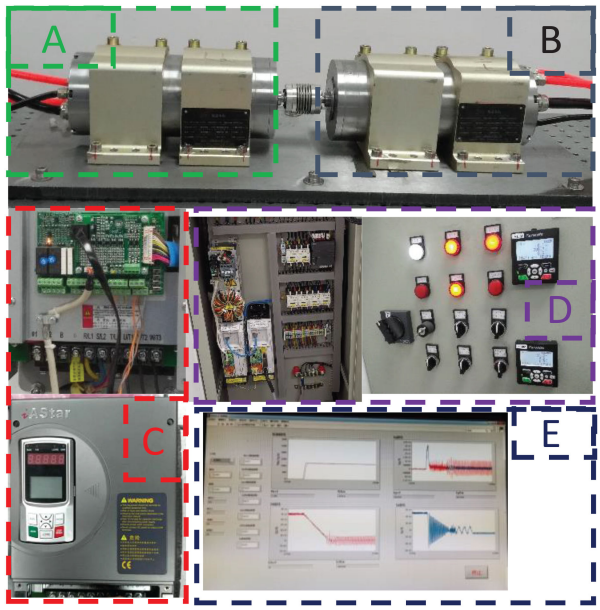

Fig. 3. The 5.5-kW PMSM platform.

where $C_{PI}(s) = K_P + K_I\frac{1}{s}$, $F_{L1}(s) = \frac{\beta_{11}+k_{11}}{s+\beta_{11}+k_{11}}$, $K_P = \frac{\beta_{11}k_{11}+\beta_{11}}{b_m(\beta_{11}+k_{11})}$, and $K_I = \frac{\beta_{21}k_{11}}{b_m(\beta_{11}+k_{11})}$.

In Fig. 2, the feedback characteristics cannot be influenced by the prefilter ($H(s)$) [43]. Thus, each first-order LADRC corresponds to a PI controller. At the same time, (29) has established the comparison criterion between the first-order LADRC and the PI controller. Equation (29) also verifies that the first-order LADRC has stronger ability in attenuating overshoot and measurement noise than that of PI controller. Thus, we do not repeat the experiment results in our article, and the similar experiment results are illustrated in [42].

Second, we try to establish the comparison criterion between the LADRC and linear–nonlinear switching ADRCs. The detailed parameter tuning rules are illustrated as follows: the gain coefficients of the linear–nonlinear switching ESO must be smaller than that of the linear ESO, which helps to verify that the performance of the proposed linear–nonlinear switching ESOs is better than that of the linear ESO.

The above comparison criterion is used to in Section VII.

TABLE I
KEY PARAMETERS OF THE HIGH SPEED PERMANENT MAGNET SYNCHRONOUS MACHINE IN NOMINAL PARAMETER CONDITION

Symbols	Description	Value	Unit
Ψ_f	flux linkage	0.0515	$V.s$
n_p	pole of pairs	1	\
R_s	stator phase resistance	0.31	Ω
L_d	inductance of d axis	0.00173	H
L_q	inductance of q axis	0.00173	H
J	moment of inertia	169.33	$kg.mm^2$

VII. EXPERIMENT RESULTS AND DISCUSSIONS

The 5.5-kW PMSM platform is shown in Fig. 3. And the corresponding technical parameters are given in Table I. A is the PMSM. C is the control system of A. The proposed linear–nonlinear switching ADRCs (namely LNSADRC type 1 and LNSADRC type 2) are downloaded into the C. The system consisting of B and D is the electric dynamometer. E is the data acquisition system, which is programmed by Labview.

The speed controller and the current controller designed by the proposed linear–nonlinear switching ADRCs are validated by the 5.5-kW PMSM platform. First, we illustrate the experiment results of speed controller. Next, the current controller experiments are shown by us.

A. Speed Controllers Experiments

b_0 is the estimated value of b_m. According to the nominal parameters of the PMSM, we can get the nominal $b_0 = 456$. When the value of b_0 deviates from the nominal value, the uncertainty on b_0 is resulted from Ψ_d and J. So, different values of b_0 are used to test the performance of the proposed ESOs.

In order to evaluate the performance of the proposed speed controllers, comparison will be made with the speed controller based on the LNSADRC type 3 in [34] and LADRC [39].

The current loop controller adopts PI algorithm, and the corresponding protection procedures, such as over-current protection and over-voltage protection, are considered. Such considerations can guarantee that the experiment is operated safely. For d–q axis PI controllers, the proportional coefficient is 7.35 and the integral coefficient is 17.15.

It also means that the parameters of the proposed linear–nonlinear switching ADRCs must be limited within a certain range. Thus, the corresponding parameters are shown as follows in consideration of the constraints in Theorems 1 and 2. Condition 1: $p = 9$, $q = 8$, $m = 2$, $n = 1$, $\beta_{21}^{(1)} = 20$, $\beta_{21}^{(2)} = 40$, $\beta_{21}^{(3)} = \frac{160}{3}$, $\beta_{11}^{(1)} = 40$, $\beta_{11}^{(2)} = 40$, $\beta_{11}^{(3)} = 60$, $\beta_{11} = 160$, $\beta_{21} = \frac{160}{3}$, $\delta_2 = \frac{64}{9} rad/s$, $\delta_1 = 1\, rad/s$, $k_{11} = 5$, $b_0 = 456 \times 0.6$. Condition 2: $p = 9$, $q = 8$, $m = 2$, $n = 1$, $\beta_{21}^{(1)} = 20$, $\beta_{21}^{(2)} = 40$, $\beta_{21}^{(3)} = \frac{160}{3}$, $\beta_{11}^{(1)} = 40$, $\beta_{11}^{(2)} = 40$, $\beta_{11}^{(3)} = 60$, $\beta_{11} = 160$, $\beta_{21} = \frac{160}{3}$, $\delta_2 = \frac{64}{9} rad/s$, $\delta_1 = 1\, rad/s$, $k_{11} = 5$, $b_0 = 456$. Condition 3: $p = 9$, $q = 8$, $m = 2$, $n = 1$, $\beta_{21}^{(1)} = 20$, $\beta_{21}^{(2)} = 40$, $\beta_{21}^{(3)} = \frac{160}{3}$, $\beta_{11}^{(1)} = 40$, $\beta_{11}^{(2)} = 40$, $\beta_{11}^{(3)} = 60$, $\beta_{11} = 160$, $\beta_{21} = \frac{160}{3}$, $\delta_2 = \frac{64}{9} rad/s$, $\delta_1 = 1\, rad/s$, $k_{11} = 5$, $b_0 = 456 \times 1.4$. Condition 4: The parameters of LADRC are as follows: $\beta_{11} = 160$, $\beta_{21} = 160/3$, $k_{11} = 5$, and $b_0 = 456$. The parameters of LADRC1 are as follows: $\beta_{11} = 160$, $\beta_{21} = 1440$, $k_{11} = 5$, and $b_0 = 456$. The parameters of LADRC2 are as follows: $\beta_{11} = 160$, $\beta_{21} = 6400$, $k_{11} = 5$, and $b_0 = 456$.

In experiment processes, the step load torque disturbance (T_L), whose magnitude is 20% of the nominal electromagnetic torque of PMSM, is applied to the PMSM by the electric dynamometer. Figs. 4–6 illustrate that the performance of LNSADRC type 1, LNSADRC type 2, and LNSADRC type 3 are superior to that of LADRC when the PMSM faces the step load torque disturbance and the uncertainty of b_0. When the load torque (T_L) is applied to the PMSM, the LNSADRC type 2 has the minimum value of speed drop, followed by the LNSADRC type 1 and the LNSADRC type 3, and the largest value of speed drop is the LADRC. When the load torque (T_L) is removed from the PMSM, the LADRC has the largest value of speed rise, and the LNSADRC type 2 has the smallest value of speed rise, and the LNSADRC type 1 and the LNSADRC type 3 rank the middle place. Thus, we can conclude that the LNSADRC type 2 has the best performance from the values of speed rise and speed drop perspective. Furthermore, when b_0 increases, the values of speed rise and speed drop go up for the LNSADRC type 1, the LNSADRC type 2, the LNSADRC type 3 and the LADRC, and the rate of change of magnitude value of speed drop is greater than that of speed rise. In Condition 1, the maximum value of speed rise of the LADRC is 27 times as large as the LNSADRC type 2, and the maximum value of speed drop of the LADRC is 32 times as big as the LNSADRC type 2. In Condition 1, the maximum value of speed rise of the LADRC is 22 times larger than the LNSADRC type 1 and the LNSADRC type 3, and the maximum value of speed drop of the LADRC is 29 times bigger than the LNSADRC type 1 and the LNSADRC type 3. In Condition 2, the maximum value of speed rise of the LADRC is 27 times as big as the LNSADRC type 2, and the maximum value of speed drop of the LADRC is 28 times as large as the LNSADRC type 2. In Condition 2, the maximum value of speed rise of the LADRC is 22 times larger than the LNSADRC type 1 and the LNSADRC type 3, and the maximum value of speed drop of the LADRC is 25 times larger than the LNSADRC type 1 and the LNSADRC type 3. In Condition 3, the maximum value of speed rise of the LADRC is 24 times as big as the LNSADRC type 2, and the maximum value of speed drop of the LADRC is 25 times as large as the LNSADRC type 2. In Condition 3, the maximum value of speed rise of the LADRC is 22 times bigger than the LNSADRC type 1 and the LNSADRC type 3, and the maximum value of speed drop of the LADRC is 23 times as big as the LNSADRC type 1 and the LNSADRC type 3.

The specific values are also illustrated in Table II, where AA, BB, CC, and DD stand for the LNSADRC type 1, the LNSADRC type 2, the LNSADRC type 3, and the LADRC, respectively.

From Figs. 4–7, the performance of LADRC can approach that of the LNSADRC type 1, the LNSADRC type 2, and the LNSADRC type 3 by increasing the gain coefficients of ESO of LADRC. However, for the LADRC2, the speed fluctuates sinusoidally when the load torque (T_L) is removed from the PMSM, which is resulted from the overlarge β_{21}. The specific values are also illustrated in Table III. The

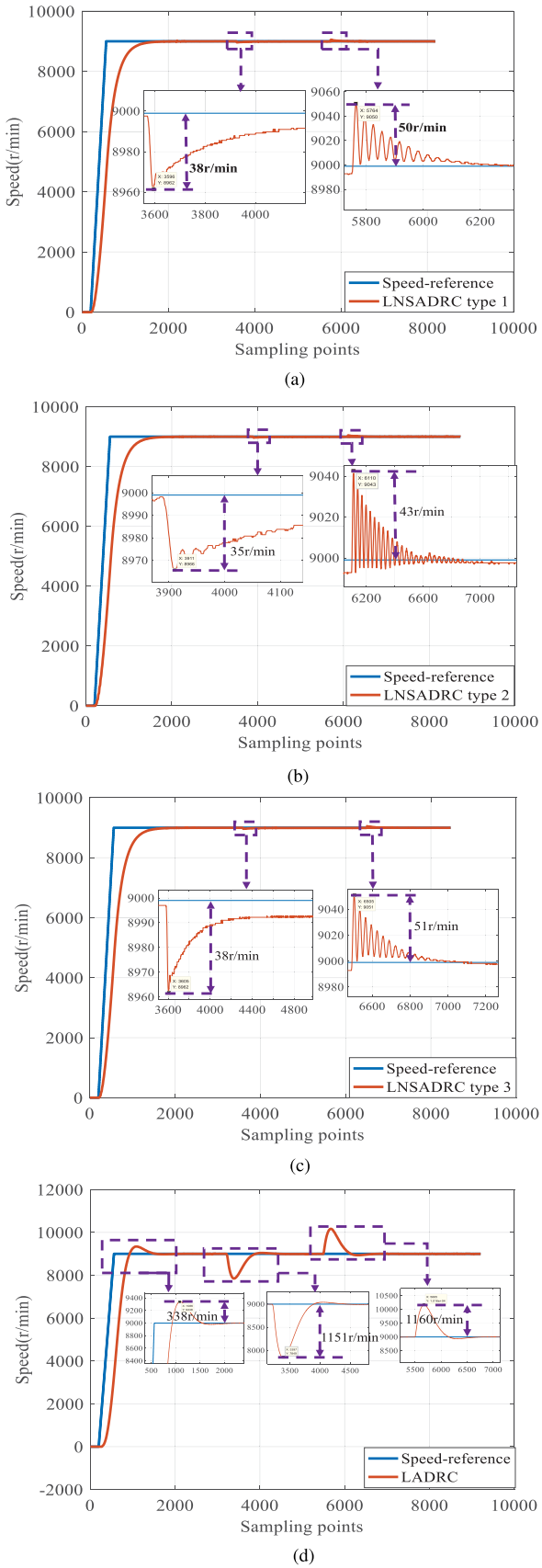

Fig. 4. Speed response of different ADRCs in Condition 1. (a) The LNSADRC type 1. (b) The LNSADRC type 2. (c) The LNSADRC type 3. (d) The LADRC.

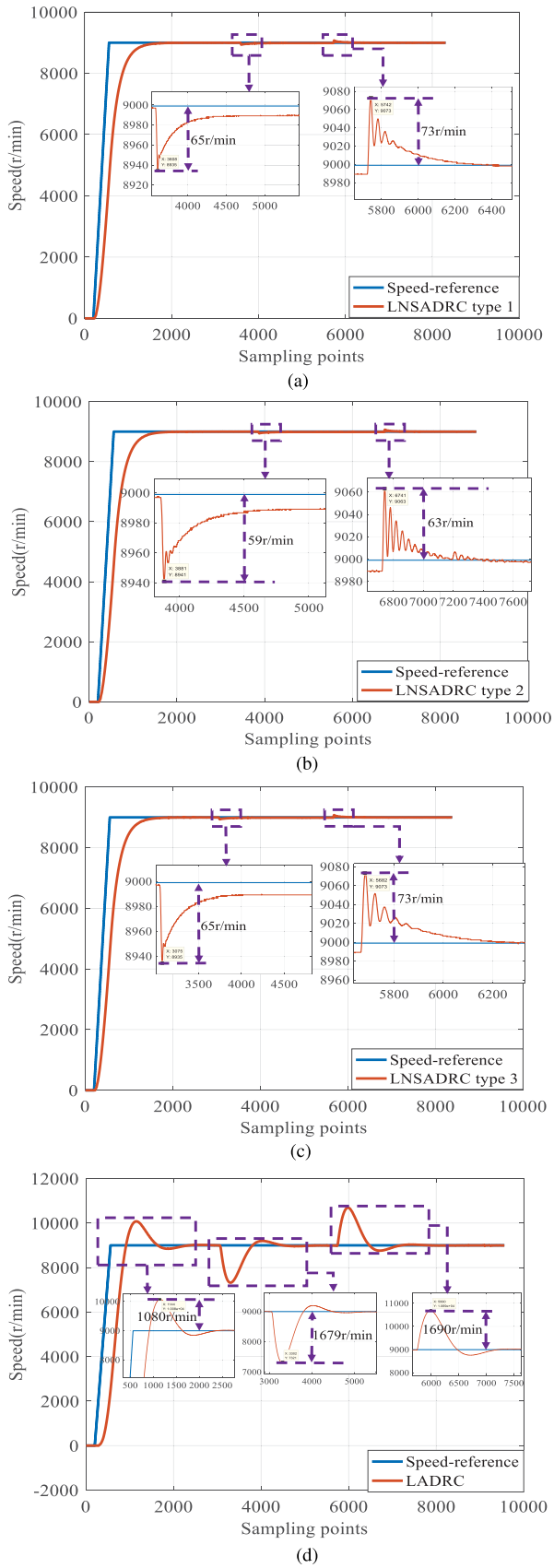

Fig. 5. Speed response of different ADRCs in Condition 2. (a) The LNSADRC type 1. (b) The LNSADRC type 2. (c) The LNSADRC type 3. (d) The LADRC.

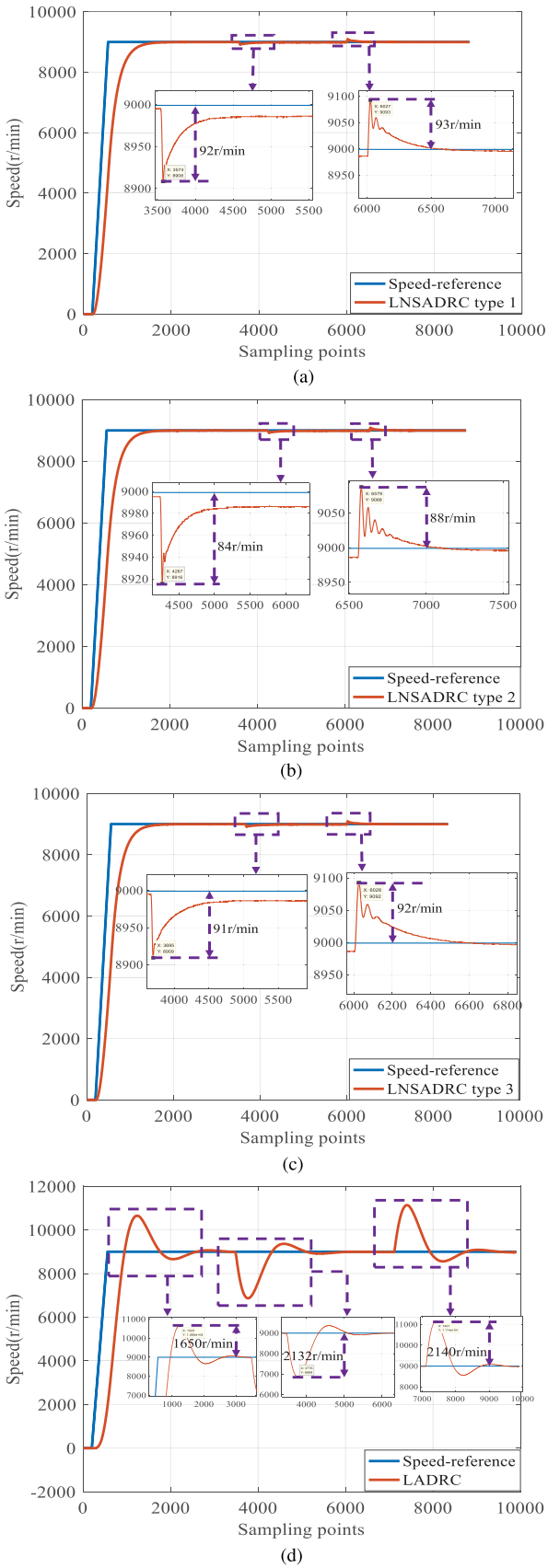

Fig. 6. Speed response of different ADRCs in Condition 3. (a) The LNSADRC type 1. (b) The LNSADRC type 2. (c) The LNSADRC type 3. (d) The LADRC.

TABLE II
SPEED VARIATION OF DIFFERENT ADRCS

Condition 1	AA	BB	CC	DD
Speed rise (r/min)	50	43	51	1160
Speed rise (%)	0.56	0.48	0.57	12.89
Speed drop (r/min)	38	35	38	1151
Speed drop (%)	0.42	0.39	0.42	12.79
Condition 2	AA	BB	CC	DD
Speed rise (r/min)	73	63	73	1690
Speed rise (%)	0.81	0.7	0.81	18.78
Speed drop (r/min)	65	59	65	1679
Speed drop (%)	0.72	0.66	0.72	18.66
Condition 3	AA	BB	CC	DD
Speed rise (r/min)	93	88	92	2140
Speed rise (%)	1.03	0.98	1.02	23.78
Speed drop (r/min)	92	84	91	2132
Speed drop (%)	1.02	0.93	1.01	23.69

TABLE III
SPEED VARIATION OF DIFFERENT LINEAR ADRCS

Condition 4	The LADRC	The LADRC1	The LADRC2
Speed rise (r/min)	1690	124	33
Speed rise (%)	18.78	1.38	0.37
Speed drop (r/min)	1679	120	25
Speed drop (%)	18.66	1.33	0.28

proposed LNSADRC type 1 and LNSADRC type 2 have small gain coefficients ($\beta_{11}^{(1)}$, $\beta_{11}^{(2)}$, $\beta_{11}^{(3)}$, $\beta_{21}^{(1)}$, $\beta_{21}^{(2)}$, $\beta_{21}^{(3)}$), which can avoid the similar problems. It also shows that switching rules adopted in estimating z_1 can decrease the gain of ESO without sacrificing the ability of disturbance rejection. The overshoot of speed response caused by improper parameter setting of LADRC, which is shown in Figs. 4(d), 5(d), 6(d), and 7(a), can be solved by the proposed linear–nonlinear switching ADRCs.

Of course, the overshoot of speed response caused by improper parameter setting of LADRC can be implemented by using the traditional methods in [39].

B. Current Controllers Experiments

The speed loop adopts LADRC controller. The q-axis current loop adopts the proposed ADRC controller. The d-axis current loop adopts the PI controller, and the proportional coefficient is 7.35 and the integral coefficient is 17.15. Condition 5: $\beta_{11} = 16$, $\beta_{21} = 144$, $k_{11} = 5$, $b_0 = 456$, $\alpha_{12} = 8/9$, $\alpha_{22} = 1/2$, $\beta_{22}^{(1)} = 160/9$, $\beta_{22}^{(2)} = 40$, $\beta_{22}^{(3)} = \frac{160}{3}$, $\beta_{12}^{(1)} = 40$, $\beta_{12}^{(2)} = 40$, $\beta_{12}^{(3)} = 60$, $\beta_{12} = 160$, $\beta_{22} = \frac{160}{3}$, $\delta_{22} = 9A$, $\delta_{12} = 4A$, $k_{12} = 60$, $b_{02} = 578$. Condition 6: $\beta_{11} = 16$, $\beta_{21} = 144$, $k_{11} = 5$, $b_0 = 456$, $\alpha_{12} = 8/9$, $\alpha_{22} = 1/2$, $\beta_{22}^{(1)} = 160/9$, $\beta_{22}^{(2)} = 40$, $\beta_{22}^{(3)} = \frac{160}{3}$, $\beta_{12}^{(1)} = 40$, $\beta_{12}^{(2)} = 40$, $\beta_{12}^{(3)} = 60$, $\beta_{12} = 160$, $\beta_{22} = \frac{160}{3}$, $\delta_{22} = 9A$, $\delta_{12} = 4A$, $k_{12} = 60$, $b_{02} = 578 \times 2$. Condition 7: $\beta_{11} = 160$, $\beta_{21} = 1440$, $k_{11} = 5$, $b_0 = 456$, $\alpha_{12} = 8/9$, $\alpha_{22} = 1/2$, $\beta_{22}^{(1)} = 160/9$, $\beta_{22}^{(2)} = 40$, $\beta_{22}^{(3)} = \frac{160}{3}$, $\beta_{12}^{(1)} = 40$, $\beta_{12}^{(2)} = 40$, $\beta_{12}^{(3)} = 60$, $\delta_{22} = 9A$, $\delta_{12} = 4A$, $k_{12} = 60$.

In order to test the tracking ability of the current controller designed by the proposed ADRCs, the output of the speed

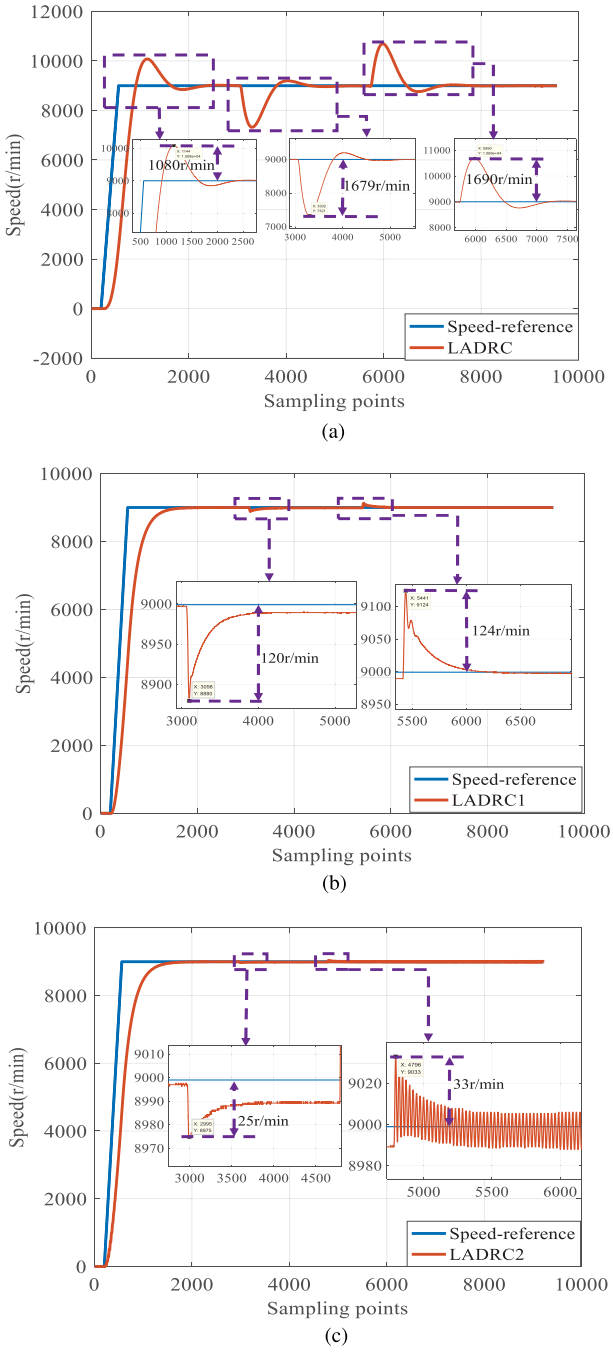

Fig. 7. Speed response of different LADRCs by changing β_{21} in Condition 4. (a) The LADRC. (b) The LADRC1. (c) The LADRC2.

controller designed by the LADRC has sinusoidal fluctuation phenomenon. The corresponding parameters are illustrated in Condition 5.

By observing the Figs. 8–10, we can obtain the following experience. The ADRCs including the LNSADRC type1, the LNSADRC type2, the LNSADRC type3, and the LADRC have good sinusoidal tracking performance. By increasing the value of b_{02}, the tracking error value of i_q is decreased for the LNSADRC type1, the LNSADRC type2, and the LNSADRC

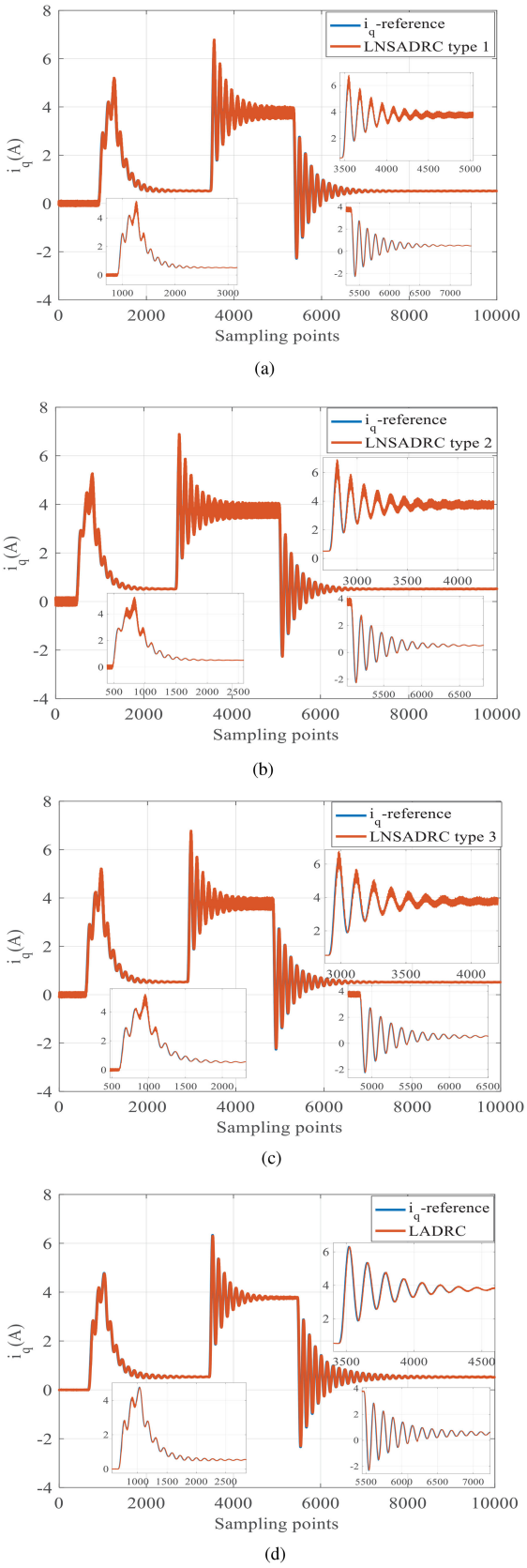

Fig. 8. i_q current response of different ADRCs in Condition 5. (a) The LNSADRC type 1. (b) The LNSADRC type 2. (c) The LNSADRC type 3. (d) The LADRC.

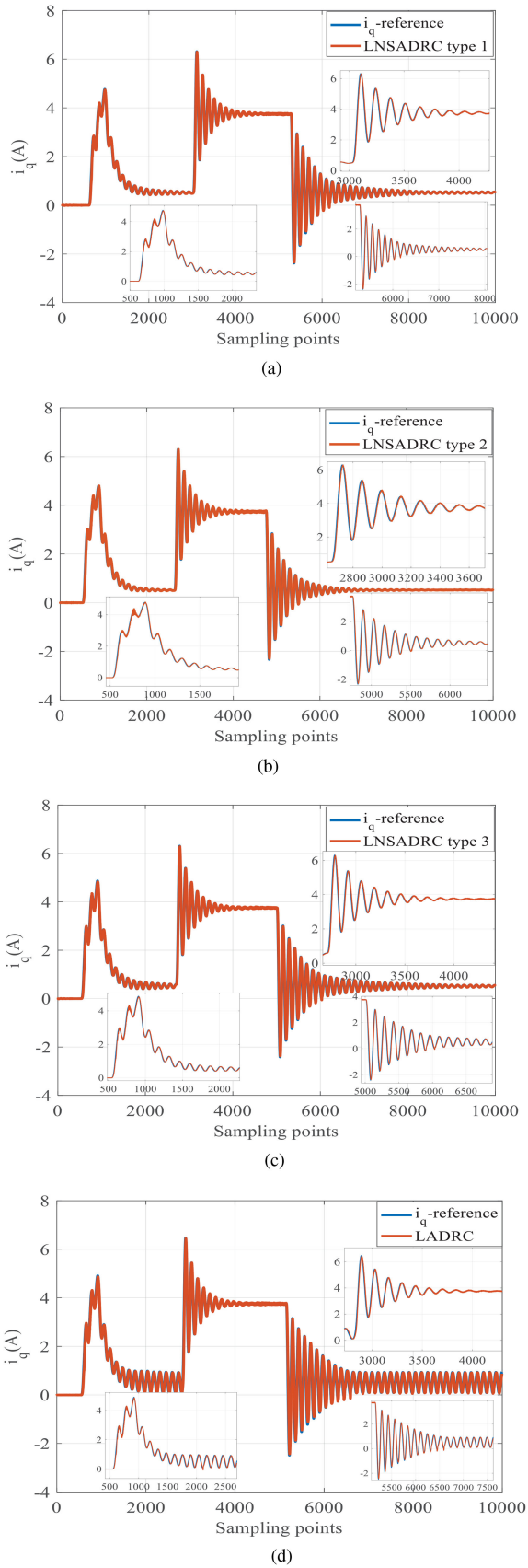

Fig. 9. i_q current response of different ADRCs in Condition 6. (a) The LNSADRC type 1. (b) The LNSADRC type 2. (c) The LNSADRC type 3. (d) The LADRC.

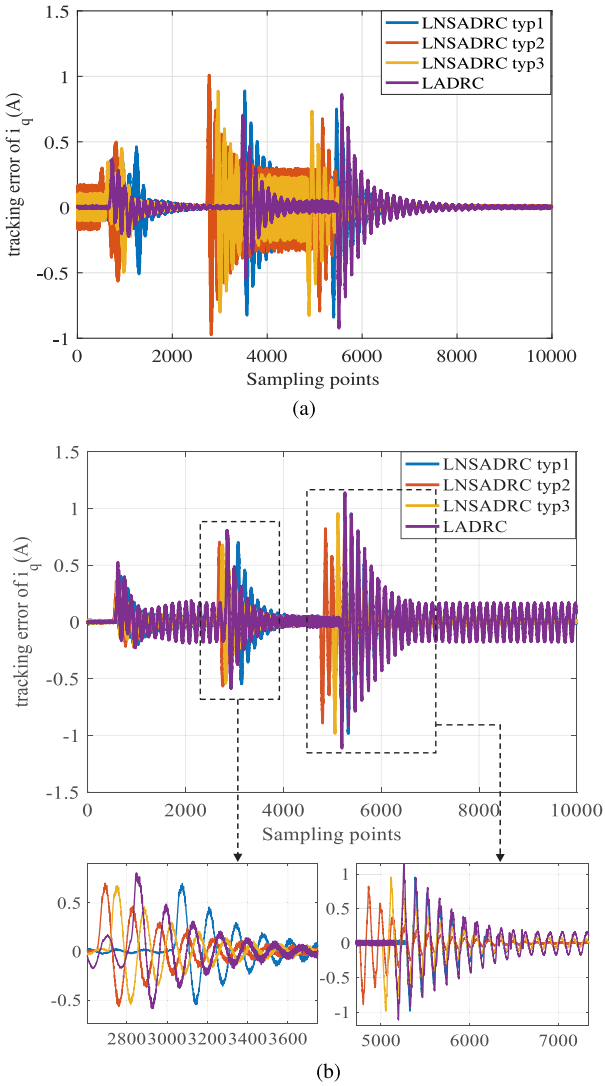

Fig. 10. Tracking error of i_q current of different ADRCs in Conditions 5 and 6. (a) Condition 5. (b) Condition 6.

type3. However, the tracking error value of i_q of the LADRC is increased. When $b_{02} = 1156$, the LNSADRC type 2 has the minimum value of tracking error of i_q. Nevertheless, the LADRC has the worst tracking performance.

We increase the gain coefficients of ESO of the LADRC in speed loop. The corresponding parameters in Condition 7 have increased to tenfold of the value in Condition 5. The experiment results of the LNSADRC type2 are illustrated in Fig. 11. By increasing the value of b_{02}, the tracking error of i_q decreases sharply. Because the parameters of the LADRC for speed loop are different in Conditions 5 and 7, the reference value of i_q (i_q-reference) is different in Figs. 8(b) and 11(a). When b_{02} deviates from the nominal value of b_q, the tracking error value of i_q for the LNSADRC type2 decreases substantially.

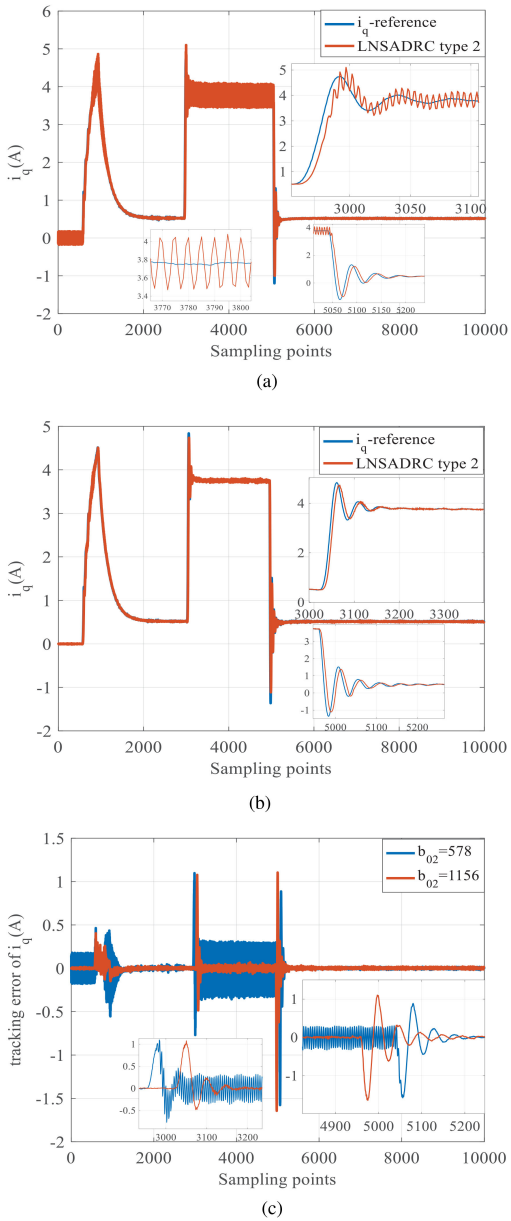

Fig. 11. i_q current response of the LNSADRC type1 in Condition 7 by changing b_{02}. (a) $b_{02} = 578$. (b) $b_{02} = 1156$. (c) The tracking error of i_q.

VIII. Conclusion

This article has investigated a class of linear–nonlinear switching ADRCs applied to design speed controller and current controller for PMSM. The stability of linear–nonlinear switching ESOs are addressed by multiple Lyapunov functions, and the stability of closed-loop systems is proved by the frequency domain method. The advantages of speed controllers and current controllers designed by the proposed linear-nonlinear switching ADRCs are validated by experiment results of a 5.5-kW PMSM platform. The experiment results of the speed controllers illustrate that the proposed ADRCs (LNSADRC type 1 and LNSADRC type 2) are more proficient in inhibiting changes of speed than the LADRC and the LNSADRC type 3 in coping with disturbances. The proposed LNSADRC type 1 and LNSADRC type 2 can overcome the overshoot of speed response caused by improper parameter setting of LADRC. The experiment results of the current controllers show that the proposed LNSADRC type 2 has better tracking ability than the LNSADRC type 1, the LNSADRC type 3, and the LADRC when b_{02} is not estimated accurately.

Appendix A
Proof of the Theorem 1

Proof: The candidate Lyapunov function $V(e)$, constituting of multiple Lyapunov functions, of system (13) can be proposed as

$$\begin{cases} V(e) = V_{13}(e), |e_1| \le \delta_1 \\ V(e) = V_{12}(e), \delta_1 < |e_1| \le \delta_2 \\ V(e) = V_{11}(e), |e_1| > \delta_2 \end{cases} \tag{30}$$

where

$$\begin{cases} V_{13} = (c_3 e_1^2 + b e_2^2)^{\frac{2m}{m+n}} + c_3 e_1^2 + b e_2^2 - a e_1 e_2 \\ V_{12} = (|e_1|^{\frac{n}{m}+1} + b e_2^2)^{\frac{2m}{m+n}} + |e_1|^{\frac{n}{m}+1} + b e_2^2 - a e_1 e_2 \\ V_{11} = (c_1 e_1^2 + b e_2^2)^{\frac{2m}{m+n}} + c_1 e_1^2 + b e_2^2 - a e_1 e_2. \end{cases}$$

The parameters of $V(e)$ satisfy $b = \frac{1}{\beta_{21}^{(3)}}$, $c_1 = \frac{\beta_{21}^{(1)}}{\beta_{21}^{(3)}}$, $c_3 = \frac{1}{\delta_1^{(1-\alpha_2)}}$, $e = [e_1, e_2]^T$, and $a \in (0, R_2)$ with $R_2 = min\{R_{21}, R_{22}, R_{23}, R_{24}, R_{25}, R_{26}\}$, where

$$R_{21} = \frac{2\beta_{11}\beta_{21}^{(1)}}{\beta_{21}^{(1)}\beta_{21}^{(3)} + \frac{1}{4}\beta_{11}^2\beta_{21}^{(3)}}, R_{22} = \frac{2\beta_{11}}{\beta_{21}^{(3)} + \frac{1}{4}\beta_{11}^2\delta_1^{(1-\alpha_2)}}$$

$$R_{23} = \frac{2\sqrt{\beta_{21}^{(1)}}}{\beta_{21}^{(3)}}, R_{24} = \frac{2}{\sqrt{\beta_{21}^{(3)}}}$$

$$R_{25} = \frac{2}{\sqrt{\beta_{21}^{(3)}\delta_1^{(1-\alpha_2)}}}, R_{26} = \frac{(m+n)\beta_{11}}{m\beta_{21}^{(2)}}.$$

By mathematical deduction, $a \in (0, R_2)$ can guarantee that (31)–(35) are true

$$\begin{bmatrix} a & -\frac{1}{2}a\beta_{11} \\ -\frac{1}{2}a\beta_{11} & \left(2\beta_{11}c_1 - \beta_{21}^{(1)}a\right) \end{bmatrix} \succ 0 \tag{31}$$

$$\begin{bmatrix} a & -\frac{a\beta_{11}}{2} \\ -\frac{a\beta_{11}}{2} & \left(-\frac{a\beta_{21}^{(3)}}{\delta_1^{1-\alpha_2}} + 2c_3\beta_{11}\right) \end{bmatrix} \succ 0 \tag{32}$$

$$\begin{bmatrix} c_1 & -\frac{a}{2} \\ -\frac{a}{2} & b \end{bmatrix} \succ 0 \tag{33}$$

$$\begin{bmatrix} 1 & -\frac{a}{2} \\ -\frac{a}{2} & b \end{bmatrix} \succ 0 \tag{34}$$

$$\begin{bmatrix} c_3 & -\frac{a}{2} \\ -\frac{a}{2} & b \end{bmatrix} \succ 0. \tag{35}$$

Step 1: By mathematical deduction, we can get $V_{11} \ge c_1 e_1^2 + b e_2^2 - a e_1 e_2$, $V_{12} \ge |e_1|^2 + b e_2^2 - a e_1 e_2$, and $V_{13} \ge c_3 e_1^2 +$

$be_2^2 - ae_1e_2$. Inequalities (33)–(35) mean that V_{1d} are positive definite and radially unbounded, where $d \in \{1, 2, 3\}$.

Step 2: We will show that the given functions do not increase during switching instants. And during continuous evolution, the function is decreasing. Computing the derivative of V_{1d} along the solution of system (13) yields that

$$\begin{aligned}\dot{V}_{13} = &\frac{2m}{m+n}(c_3e_1^2+be_2^2)^{\frac{2m}{m+n}-1}\Bigg[2c_3e_1e_2-2c_3\beta_{11}e_1^2\\&+2be_2h-2b\frac{\beta_{21}^{(3)}e_1e_2}{\delta_1^{1-\alpha_1}}\Bigg]+2c_3e_1e_2-2c_3\beta_{11}e_1^2\\&+2be_2h-2b\frac{\beta_{21}^{(3)}e_1e_2}{\delta_1^{1-\alpha_1}}-ae_2^2\\&+\beta_{11}ae_2e_1-ae_1h+\frac{\beta_{21}^{(3)}ae_1^2}{\delta_1^{1-\alpha_1}}\end{aligned} \tag{36}$$

$$\begin{aligned}\dot{V}_{12} = &\frac{2m}{m+n}(|e_1|^{\frac{n}{m}+1}+be_2^2)^{\frac{m-n}{m+n}}[\frac{m+n}{m}|e_1|^{\frac{n}{m}}e_2sign(e_1)\\&-\frac{m+n}{m}|e_1|^{\frac{n}{m}+1}\beta_{11}+2be_2h-2b\beta_{21}^{(2)}|e_1|^{\frac{n}{m}}e_2sign(e_1)]\\&+\frac{m+n}{m}|e_1|^{\frac{n}{m}}e_2sign(e_1)-\frac{m+n}{m}|e_1|^{\frac{n}{m}+1}\beta_{11}\\&+2be_2h-2be_2\beta_{21}^{(2)}|e_1|^{\frac{n}{m}}sign(e_1)\\&-ae_2^2+\beta_{11}ae_1e_2-ae_1h+a\beta_{21}^{(2)}|e_1|^{\frac{n}{m}+1}\end{aligned} \tag{37}$$

$$\begin{aligned}\dot{V}_{11} = &\frac{2m}{m+n}(c_1e_1^2+be_2^2)^{\frac{2m}{m+n}-1}[2c_1e_1e_2\\&-\beta_{11}2c_1e_1^2+2be_2h-\beta_{21}^{(1)}2be_2e_1]\\&+[2c_1e_1e_2-\beta_{11}2c_1e_1^2+2be_2h-\beta_{21}^{(1)}2be_2e_1]\\&-ae_2^2+\beta_{11}ae_2e_1-ae_1h+a\beta_{21}^{(1)}e_1^2.\end{aligned} \tag{38}$$

The inequality (31) results in $-ae_2^2+a\beta_{11}^{(1)}e_1e_2-(2\beta_{11}^{(1)}c_1-\beta_{21}^{(1)}a)e_1^2<0$. And when $c_1=\beta_{21}^{(1)}b$, (38) can be recast as

$$\begin{aligned}\dot{V}_{11} = &-\beta_{11}2c_1e_1^2\frac{2m}{m+n}(c_1e_1^2+be_2^2)^{\frac{2m}{m+n}-1}-ae_2^2\\&+\beta_{11}ae_2e_1-(2\beta_{11}c_1-a\beta_{21}^{(1)})e_1^2\\&+2be_2h\frac{2m}{m+n}(c_1e_1^2+be_2^2)^{\frac{2m}{m+n}-1}+2be_2h-ae_1h.\end{aligned} \tag{39}$$

It is easy to derive the following inequality:

$$(c_1e_1^2+be_2^2)^{\frac{2m}{m+n}-1}\le(2c_1e_1^2)^{\frac{2m}{m+n}-1}+(2be_2^2)^{\frac{2m}{m+n}-1} \tag{40}$$

and then we have

$$e_2(c_1e_1^2+be_2^2)^{\frac{2m}{m+n}-1}\le|e_2|(2c_1e_1^2)^{\frac{2m}{m+n}-1}+|e_2|(2be_2^2)^{\frac{2m}{m+n}-1}. \tag{41}$$

Furthermore, the inequality (41) can be recast as

$$\begin{aligned}e_2(c_1e_1^2+be_2^2)^{\frac{2m}{m+n}-1}\le&|e_2|(|e_1|)^{2\frac{2m}{m+n}-2}(2c_1)^{\frac{2m}{m+n}-1}\\&+|e_2|^{2\frac{2m}{m+n}-1}(2b)^{\frac{2m}{m+n}-1}.\end{aligned} \tag{42}$$

By combining (39) and inequality (42), one can conclude that

$$\begin{aligned}\dot{V}_{11}\le&-\beta_{11}2c_1e_1^2\frac{2m}{m+n}(c_1e_1^2+be_2^2)^{\frac{2m}{m+n}-1}-ae_2^2\\&+\beta_{11}ae_2e_1-(2\beta_{11}c_1-a\beta_{21}^{(1)})e_1^2\\&+2bR_1[|e_2|(|e_1|)^{2\frac{2m}{m+n}-2}(2c_1)^{\frac{2m}{m+n}-1}\\&+|e_2|^{2\frac{2m}{m+n}-1}(2b)^{\frac{2m}{m+n}-1}]+2be_2h-ae_1h.\end{aligned} \tag{43}$$

The constraint $m<3n$ results in $2\frac{2m}{m+n}-2<1$ and $2\frac{2m}{m+n}-1<2$. Toward that end, the order of the negative terms is larger than the order of the positive terms in (45). Then with the constraint $0<\theta_{11}<1$, thus, the following result can be obtained:

$$\begin{aligned}\dot{V}_{11}\le&-(1-\theta_{11})[\beta_{11}2c_1e_1^2\frac{2m}{m+n}(c_1e_1^2+be_2^2)^{\frac{2m}{m+n}-1}\\&+ae_2^2-\beta_{11}ae_2e_1+(2\beta_{11}c_1-a\beta_{21}^{(1)})e_1^2]\end{aligned} \tag{44}$$

when

$$\begin{aligned}g_{11}=&-\theta_{11}[\beta_{11}2c_1e_1^2\frac{2m}{m+n}(c_1e_1^2+be_2^2)^{\frac{2m}{m+n}-1}\\&+ae_2^2-\beta_{11}ae_2e_1+(2\beta_{11}c_1-a\beta_{21}^{(1)})e_1^2]\\&+2bR_1[|e_2|(|e_1|)^{2\frac{2m}{m+n}-2}(2c_1)^{\frac{2m}{m+n}-1}\\&+|e_2|^{2\frac{2m}{m+n}-1}(2b)^{\frac{2m}{m+n}-1}]+2be_2h-ae_1h\le0.\end{aligned} \tag{45}$$

And when $\frac{m+n}{m}=\beta_{21}^{(2)}2b$ and $\frac{m+n}{m\beta_{21}^{(2)}}\beta_{11}>a$, (37) can be recast as

$$\begin{aligned}\dot{V}_{12}\le&-2(|e_1|^{\frac{n}{m}+1}+be_2^2)^{\frac{m-n}{m+n}}|e_1|^{\frac{n}{m}+1}\beta_{11}-ae_2^2\\&+\frac{2m}{m+n}(|e_1|^{\frac{n}{m}+1}+be_2^2)^{\frac{m-n}{m+n}}2be_2h\\&+2be_2h+\beta_{11}ae_1e_2-ae_1h.\end{aligned} \tag{46}$$

It is easy to verify the following inequality:

$$\begin{aligned}(|e_1|^{\frac{n}{m}+1}+be_2^2)^{\frac{m-n}{m+n}}&\le(2|e_1|^{\frac{n}{m}+1})^{\frac{m-n}{m+n}}+(2be_2^2)^{\frac{m-n}{m+n}}\\&=(|e_1|)^{\frac{m-n}{m}}2^{\frac{m-n}{m+n}}+(e_2)^{\frac{2(m-n)}{m+n}}(2b)^{\frac{m-n}{m+n}}.\end{aligned} \tag{47}$$

Thus, one can conclude that

$$\begin{aligned}e_2(|e_1|^{\frac{n}{m}+1}+be_2^2)^{\frac{m-n}{m+n}}\le&|e_2||e_1|^{\frac{m-n}{m}}2^{\frac{m-n}{m+n}}\\&+|e_2|^{\frac{2(m-n)}{m+n}+1}(2b)^{\frac{m-n}{m+n}}.\end{aligned} \tag{48}$$

With the constraints $3n>m$ and inequality (48), the order of the negative terms is larger than the order of the positive terms in (50). With $0<\theta_{12}<1$, we have

$$\dot{V}_{12}\le-(1-\theta_{12})[2(|e_1|^{\frac{n}{m}+1}+be_2^2)^{\frac{m-n}{m+n}}|e_1|^{\frac{n}{m}+1}\beta_{11}+ae_2^2] \tag{49}$$

when

$$\begin{aligned} g_{12} = & -\theta_{12}[2(|e_1|^{\frac{n}{m}+1}+be_2^2)^{\frac{m-n}{m+n}}|e_1|^{\frac{n}{m}+1}\beta_{11} \\ & + ae_2^2] + \frac{2m}{m+n}(|e_1|^{\frac{n}{m}+1}+be_2^2)^{\frac{m-n}{m+n}}2be_2h \\ & + 2be_2h + \beta_{11}ae_1e_2 - ae_1h \le 0. \end{aligned} \tag{50}$$

With the constraints $c_3=\frac{b\beta_{21}^{(3)}}{\delta_1^{1-\alpha_2}}$ and inequality (32), the following results can be obtained:

$$\begin{aligned} \dot{V}_{13} = & -2c_3\beta_{11}e_1^2\frac{2m}{m+n}(c_3e_1^2+be_2^2)^{\frac{2m}{m+n}-1} \\ & - ae_2^2 + \beta_{11}ae_2e_1 - \left(-\frac{\beta_{21}^{(3)}a}{\delta_1^{1-\alpha_1}} + 2c_3\beta_{11}\right)e_1^2 \\ & + 2be_2h\frac{2m}{m+n}(c_3e_1^2+be_2^2)^{\frac{2m}{m+n}-1} - ae_1h + 2be_2h. \end{aligned} \tag{51}$$

There exists

$$(c_3e_1^2+be_2^2)^{\frac{2m}{m+n}-1} \le (2c_3e_1^2)^{\frac{2m}{m+n}-1} + (2be_2^2)^{\frac{2m}{m+n}-1}. \tag{52}$$

One can conclude that

$$\begin{aligned} e_2(c_3e_1^2+be_2^2)^{\frac{2m}{m+n}-1} \le & |e_2|(e_1)^{2\frac{2m}{m+n}-2}(2c_3)^{\frac{2m}{m+n}-1} \\ & + (|e_2|)^{2\frac{2m}{m+n}-1}(2b)^{\frac{2m}{m+n}-1}. \end{aligned} \tag{53}$$

The constraint $m<3n$ results in $2\frac{2m}{m+n}-2<1$ and $2\frac{2m}{m+n}-1<2$. Thus, the inequality (53) can be recast as

$$e_2(c_3e_1^2+be_2^2)^{\frac{2m}{m+n}-1} < |e_2||e_1|(2c_3)^{\frac{2m}{m+n}-1} + |e_2|^2(2b)^{\frac{2m}{m+n}-1}. \tag{54}$$

Toward that end, the order of the negative terms is larger than the order of the positive terms in (56). With $0<\theta_{13}<1$, it holds that

$$\begin{aligned} \dot{V}_{13} \le & -(1-\theta_{13})\Bigg[2c_3\beta_{11}e_1^2\frac{2m}{m+n}(c_3e_1^2+be_2^2)^{\frac{2m}{m+n}-1} \\ & + ae_2^2 - \beta_{11}ae_2e_1 + \left(-\frac{\beta_{21}^{(3)}a}{\delta_1^{1-\alpha_1}} + 2c_3\beta_{11}\right)e_1^2\Bigg] \end{aligned} \tag{55}$$

when

$$\begin{aligned} g_{13} = & -\theta_{13}\Bigg[2c_3\beta_{11}e_1^2\frac{2m}{m+n}(c_3e_1^2+be_2^2)^{\frac{2m}{m+n}-1} \\ & + ae_2^2 - \beta_{11}ae_2e_1 + \left(-\frac{\beta_{21}^{(3)}a}{\delta_1^{1-\alpha_1}} + 2c_3\beta_{11}\right)e_1^2] \\ & + 2be_2h\frac{2m}{m+n}(c_3e_1^2+be_2^2)^{\frac{2m}{m+n}-1} - ae_1h + 2be_2h \le 0. \end{aligned} \tag{56}$$

At the switching points, $c_1=|\delta_2|^{\frac{n}{m}-1}$ according to $|\delta_2|^{\frac{n}{m}-1}$ and $c_1=\frac{\beta_{21}^{(1)}}{\beta_{21}^{(3)}}$, and $c_3=|\delta_1|^{\frac{n}{m}-1}$ according to $c_3=\frac{1}{\delta_1^{1-\alpha_2}}$ and $\alpha_2=\frac{n}{m}$, can guarantee $V_{11}=V_{12}$ and $V_{13}=V_{12}$, respectively.

The detailed deduction is illustrated as follows:

When $|e_1|=\delta_2, c_1=\frac{\beta_{21}^{(1)}}{\beta_{21}^{(3)}}$ and $|\delta_2|^{\frac{n}{m}-1}=\frac{\beta_{21}^{(1)}}{\beta_{21}^{(3)}}$ can get $V_{11}=(|e_1|^{\frac{n}{m}+1}+be_2^2)^{\frac{2m}{m+n}}+|e_1|^{\frac{n}{m}+1}+be_2^2-ae_1e_2$. Then, we define $V_{12}=(|e_1|^{\frac{n}{m}+1}+be_2^2)^{\frac{2m}{m+n}}+|e_1|^{\frac{n}{m}+1}+be_2^2-ae_1e_2$. Thus, $V_{12}=V_{11}$.

When $|e_1|=\delta_1, c_3=|\delta_1|^{\frac{n}{m}-1}$, we can obtain $V_{13}=(|e_1|^{\frac{n}{m}+1}+be_2^2)^{\frac{2m}{m+n}}+|e_1|^{\frac{n}{m}+1}+be_2^2-ae_1e_2$. $V_{12}=(|e_1|^{\frac{n}{m}+1}+be_2^2)^{\frac{2m}{m+n}}+|e_1|^{\frac{n}{m}+1}+be_2^2-ae_1e_2$ is defined by us, so we can get $V_{12}=V_{13}$.

When $V(e)\ge K$ for some $K>0, g_{11}\le 0, g_{12}\le 0, g_{13}\le 0$, and thus, $\dot{V}\le -\tilde{\alpha}(|x|)$ where $\tilde{\alpha}$ is a positive function. The proof of Theorem 1 is finished.

APPENDIX B
PROOF OF THE THEOREM 2

Proof: The candidate Lyapunov function $V(e)$, constituting of multiple Lyapunov functions, of system (16) is constructed as follows:

$$\begin{cases} V(e)=V_{23}(e), |e_1|\le\delta_1 \\ V(e)=V_{22}(e), \delta_1<|e_1|\le\delta_2 \\ V(e)=V_{21}(e), |e_1|>\delta_2 \end{cases} \tag{57}$$

where

$$\begin{cases} V_{23}=(c_3e_1^2+be_2^2)^{\frac{2m}{(m+n)}}+c_3e_1^2+be_2^2-ae_1e_2 \\ V_{22}=(|e_1|^{\frac{n}{m}+1}+be_2^2)^{\frac{2m}{(m+n)}}+|e_1|^{\frac{n}{m}+1}+be_2^2-ae_1e_2 \\ V_{21}=(c_1e_1^2+be_2^2)^{\frac{2m}{(m+n)}}+c_1e_1^2+be_2^2-ae_1e_2. \end{cases}$$

The parameters of $V(e)$ satisfy $b=\frac{1}{\beta_{21}^{(3)}}$, $c_1=\frac{\beta_{21}^{(1)}}{\beta_{21}^{(3)}}$, $c_3=\frac{1}{\delta_1^{(1-\alpha_2)}}$, $e=[e_1,e_2]^T$ and $a\in(0,R_3)$ with $R_3=min\{R_{31},R_{32},R_{33},R_{34},R_{35}\}$, where

$$R_{31}=\frac{2\beta_{11}^{(1)}\beta_{21}^{(1)}}{\beta_{21}^{(1)}\beta_{21}^{(3)}+\frac{1}{4}[\beta_{11}^{(1)}]^2\beta_{21}^{(3)}}, R_{32}=\frac{8\beta_{11}^{(3)}\delta_1^{(\alpha_1-\alpha_2)}}{4\beta_{21}^{(3)}\delta_1^{(1-\alpha_2)}+[\beta_{11}^{(3)}]^2}$$

$$R_{33}=\frac{2\sqrt{\beta_{21}^{(1)}}}{\beta_{21}^{(3)}}, R_{34}=\frac{2}{\sqrt{\beta_{21}^{(3)}}}, R_{35}=\frac{2}{\sqrt{\beta_{21}^{(3)}\delta_1^{(1-\alpha_2)}}}.$$

By mathematical deduction, $a\in(0,R_3)$ can guarantee that the following inequalities hold:

$$\begin{bmatrix} a & -\frac{1}{2}a\beta_{11}^{(1)} \\ -\frac{1}{2}a\beta_{11}^{(1)} & (2\beta_{11}^{(1)}c_1-\beta_{21}^{(1)}a) \end{bmatrix} \succ 0 \tag{58}$$

$$\begin{bmatrix} a & -\frac{a\beta_{11}^{(3)}}{2\delta_1^{1-\alpha_1}} \\ -\frac{a\beta_{11}^{(3)}}{2\delta_1^{1-\alpha_1}} & (-\frac{a\beta_{21}^{(3)}}{\delta_1^{1-\alpha_2}}+\frac{2c_3\beta_{11}^{(3)}}{\delta_1^{1-\alpha_1}}) \end{bmatrix} \succ 0 \tag{59}$$

$$\begin{bmatrix} c_1 & -\frac{a}{2} \\ -\frac{a}{2} & b \end{bmatrix} \succ 0 \tag{60}$$

$$\begin{bmatrix} 1 & -\frac{a}{2} \\ -\frac{a}{2} & b \end{bmatrix} \succ 0 \tag{61}$$

$$\begin{bmatrix} c_3 & -\frac{a}{2} \\ -\frac{a}{2} & b \end{bmatrix} \succ 0. \tag{62}$$

Step 1: By mathematical deduction, we can get $V_{21} \geq c_1 e_1^2 + be_2^2 - ae_1e_2$, $V_{22} \geq |e_1|^2 + be_2^2 - ae_1e_2$ and $V_{23} \geq c_3 e_1^2 + be_2^2 - ae_1e_2$. Inequalities (60)–(62) mean that V_{2d} are positive definite and radially unbounded, where $d \in \{1, 2, 3\}$.

*Step 2:*We will show that the given functions do not increase during switching instants. And during continuous evolution, the function is decreasing.

Computing the derivative of V_{2d} along the solution of system (16) yields that

$$\begin{aligned}\dot{V}_{23} = & \frac{2m}{(m+n)}(c_3e_1^2 + be_2^2)^{\frac{2m}{(m+n)}-1}[2c_3e_1e_2 \\ & - 2c_3\beta_{11}^{(3)}\frac{e_1^2}{\delta_1^{1-\alpha_1}} + 2be_2h - 2b\beta_{21}^{(3)}\frac{e_1e_2}{\delta_1^{1-\alpha_2}}] \\ & + [2c_3e_1e_2 - 2c_3\beta_{11}^{(3)}\frac{e_1^2}{\delta_1^{1-\alpha_1}} + 2be_2h - 2b_3\beta_{21}^{(3)}\frac{e_1e_2}{\delta_1^{1-\alpha_2}}] \\ & - ae_2e_2 + a\beta_{11}^{(3)}\frac{e_1e_2}{\delta_1^{1-\alpha_1}} - ae_1h + a\beta_{21}^{(3)}\frac{e_1^2}{\delta_1^{1-\alpha_2}}\end{aligned} \tag{63}$$

$$\begin{aligned}\dot{V}_{22} = & \frac{2m}{(m+n)}(|e_1|^{\frac{n}{m}+1} + be_2^2)^{\frac{2m}{(m+n)}-1} \\ & \times \{\frac{m+n}{m}|e_1|^{\frac{n}{m}}e_2 sign(e_1) - \beta_{11}^{(2)}|e_1|^{\frac{q}{p}}\frac{m+n}{m}|e_1|^{\frac{n}{m}} \\ & + 2be_2h - \beta_{21}^{(2)}2be_2|e_1|^{\frac{n}{m}}sign(e_1)\} \\ & + \{\frac{m+n}{m}|e_1|^{\frac{n}{m}}e_2 sign(e_1) - \frac{m+n}{m}\beta_{11}^{(2)}|e_1|^{\frac{n}{m}+\frac{q}{p}} \\ & + 2be_2h - \beta_{21}^{(2)}2be_2|e_1|^{\frac{n}{m}}sign(e_1)\} \\ & - ae_2^2 + a\beta_{11}^{(2)}|e_1|^{\frac{q}{p}}e_2 sign(e_1) - ae_1h + \beta_{21}^{(2)}a|e_1|^{\frac{n}{m}+1}\end{aligned} \tag{64}$$

$$\begin{aligned}\dot{V}_{21} = & \frac{2m}{(m+n)}(c_1e_1^2 + be_2^2)^{\frac{2m}{(m+n)}-1}[(2c_1e_1e_2 - 2\beta_{11}^{(1)}c_1e_1^2) \\ & + (2be_2h - 2\beta_{21}^{(1)}be_2e_1)] + [(2c_1e_1e_2 - 2\beta_{11}^{(1)}c_1e_1^2) \\ & + (2be_2h - 2\beta_{21}^{(1)}be_2e_1)] - ae_2^2 + a\beta_{11}^{(1)}e_1e_2 - ae_1h + \beta_{21}^{(1)}ae_1^2.\end{aligned} \tag{65}$$

The inequality (58) results in $-ae_2^2 + a\beta_{11}^{(1)}e_1e_2 - (2\beta_{11}^{(1)}c_1 - \beta_{21}^{(1)}a)e_1^2 < 0$. When $c_1 = \beta_{21}^{(1)}b$, (65) can be recast as

$$\begin{aligned}\dot{V}_{21} = & \frac{2m}{(m+n)}(c_1e_1^2 + be_2^2)^{\frac{2m}{(m+n)}-1}[-2\beta_{11}^{(1)}c_1e_1^2 + 2be_2h] \\ & + 2be_2h - ae_1h - ae_2^2 + a\beta_{11}^{(1)}e_1e_2 - (2\beta_{11}^{(1)}c_1 - \beta_{21}^{(1)}a)e_1^2.\end{aligned} \tag{66}$$

It is easy to derive

$$e_2(c_1e_1^2 + be_2^2)^{\frac{2m}{(m+n)}-1} \leq |e_2|(2c_1e_1^2)^{\frac{2m}{(m+n)}-1} + |e_2|(2be_2^2)^{\frac{2m}{(m+n)}-1}. \tag{67}$$

Furthermore, we can have

$$\begin{aligned}e_2(c_1e_1^2 + be_2^2)^{\frac{2m}{(m+n)}-1} \leq & |e_2||e_1|^{\frac{2(m-n)}{m+n}}(2c_1)^{\frac{m-n}{m+n}} \\ & + |e_2|^{\frac{3m-n}{m+n}}(2b)^{\frac{m-n}{m+n}}.\end{aligned} \tag{68}$$

Then the constraint $m < 3n$ results in $\frac{1}{2} > \frac{2m}{(m+n)} - 1 > 0$ and $3 > \frac{4m}{(m+n)}$, and $0 < \theta_{21} < 1$ and the inequality (68), the order of the negative terms is larger than the order of the positive terms in (70). Thus, the following result can be obtained:

$$\begin{aligned}\dot{V}_{21} \leq & -(1-\theta_{21})[2\beta_{11}^{(1)}c_1e_1^2\frac{2m}{m+n}(c_1e_1^2 + be_2^2)^{\frac{m-n}{m+n}} \\ & + ae_2^2 - a\beta_{11}^{(1)}e_1e_2 + (2\beta_{11}^{(1)}c_1 - \beta_{21}^{(1)}a)e_1^2]\end{aligned} \tag{69}$$

when

$$\begin{aligned}g_{21} = & -\theta_{21}[2\beta_{11}^{(1)}c_1e_1^2\frac{2m}{m+n}(c_1e_1^2 + be_2^2)^{\frac{m-n}{m+n}} \\ & + ae_2^2 - a\beta_{11}^{(1)}e_1e_2 + (2\beta_{11}^{(1)}c_1 - \beta_{21}^{(1)}a)e_1^2] \\ & + 2be_2h\frac{2m}{m+n}(c_1e_1^2 + be_2^2)^{\frac{m-n}{m+n}} + 2be_2h - ae_1h \leq 0.\end{aligned} \tag{70}$$

When $\frac{m+n}{m} = 2\beta_{21}^{(2)}b$, (64) can be recast as

$$\begin{aligned}\dot{V}_{22} = & -\beta_{11}^{(2)}2(|e_1|^{\frac{n}{m}+1} + be_2^2)^{\frac{2m}{(m+n)}-1}|e_1|^{\frac{n}{m}+\frac{q}{p}} \\ & + \frac{2m}{(m+n)}(|e_1|^{\frac{n}{m}+1} + be_2^2)^{\frac{2m}{(m+n)}-1}2be_2h \\ & - \frac{m+n}{m}\beta_{11}^{(2)}|e_1|^{\frac{n}{m}+\frac{q}{p}} + 2be_2h - ae_2^2 \\ & + a\beta_{11}^{(2)}|e_1|^{\frac{q}{p}}e_2 sign(e_1) - ae_1h + \beta_{21}^{(2)}a|e_1|^{\frac{n}{m}+1}.\end{aligned} \tag{71}$$

Using Young's inequality leads to $|a\beta_{11}^{(2)}|e_1|^{\frac{q}{p}}e_2 sign(e_1)| \leq \frac{1}{2}k_1|a\beta_{11}^{(2)}||e_1|^{2\frac{q}{p}} + \frac{1}{2k_1}|a\beta_{11}^{(2)}|e_2^2$, with $k_1 > 0$. One can conclude that

$$\begin{aligned}\dot{V}_{22} \leq & -\beta_{11}^{(2)}2(|e_1|^{\frac{n}{m}+1} + be_2^2)^{\frac{2m}{(m+n)}-1}|e_1|^{\frac{n}{m}+\frac{q}{p}} \\ & + \frac{2m}{(m+n)}(|e_1|^{\frac{n}{m}+1} + be_2^2)^{\frac{2m}{(m+n)}-1}2be_2h \\ & - \frac{m+n}{m}\beta_{11}^{(2)}|e_1|^{\frac{n}{m}+\frac{q}{p}} + 2be_2h - ae_2^2 + \frac{1}{2}k_1\left|a\beta_{11}^{(2)}\right||e_1|^{2\frac{q}{p}} \\ & + \frac{1}{2k_1}\left|a\beta_{11}^{(2)}\right|e_2^2 - ae_1h + \beta_{21}^{(2)}a|e_1|^{\frac{n}{m}+1}.\end{aligned} \tag{72}$$

With

$$(|e_1|^{\frac{n}{m}+1}+be_2^2)^{\frac{2m}{(m+n)}-1} \le (2|e_1|^{\frac{n}{m}+1})^{\frac{2m}{(m+n)}-1} + (2be_2^2)^{\frac{2m}{(m+n)}-1}$$

we can have

$$\begin{aligned}\dot{V}_{22} \le & -\beta_{11}^{(2)}2(|e_1|^{\frac{n}{m}+1}+be_2^2)^{\frac{2m}{(m+n)}-1}|e_1|^{\frac{n}{m}+\frac{q}{p}} \\ & +[\frac{2m}{(m+n)}(2|e_1|^{\frac{n}{m}+1})^{\frac{2m}{(m+n)}-1}2be_2h \\ & +\frac{2m}{(m+n)}(be_2^2)^{\frac{2m}{(m+n)}-1}2be_2h]-\frac{m+n}{m}\beta_{11}^{(2)}|e_1|^{\frac{n}{m}+\frac{q}{p}} \\ & +2be_2h-ae_2^2+\frac{1}{2}k_1\left|a\beta_{11}^{(2)}\right||e_1|^{2\frac{q}{p}} \\ & +\frac{1}{2k_1}\left|a\beta_{11}^{(2)}\right|e_2^2-ae_1h+\beta_{21}^{(2)}a|e_1|^{\frac{n}{m}+1}.\end{aligned} \tag{73}$$

Using Young's inequality, we have $\frac{2hmb}{(m+n)}2(2|e_1|^{\frac{n}{m}+1})^{\frac{2m}{(m+n)}-1}e_2 \le \frac{2hmb}{(m+n)}\frac{1}{k_2}e_2^2 + \frac{2hmb}{(m+n)}k_2[2(2|e_1|^{\frac{n}{m}+1})^{\frac{2m}{(m+n)}-1}]^2$ which satisfies $k_2>0$. Because $\frac{2n}{m}+\frac{q}{p}>1$, we have $2(\frac{n}{m}+1)(\frac{2m}{(m+n)}-1) < (\frac{n}{m}+1)(\frac{2m}{(m+n)}-1)+\frac{n}{m}+\frac{q}{p}$. And $0<\theta_{22}<1$.

Then the following results can be obtained:

$$\begin{aligned}\dot{V}_{22} \le & -(1-\theta_{22})\{\beta_{11}^{(2)}2(|e_1|^{\frac{n}{m}+1}+be_2^2)^{\frac{2m}{(m+n)}-1}|e_1|^{\frac{n}{m}+\frac{q}{p}} \\ & +\frac{m+n}{m}\beta_{11}^{(2)}|e_1|^{\frac{n}{m}+\frac{q}{p}}+ae_2^2\} \\ & -\theta_{22}\{\beta_{11}^{(2)}2(|e_1|^{\frac{n}{m}+1}+be_2^2)^{\frac{2m}{(m+n)}-1}|e_1|^{\frac{n}{m}+\frac{q}{p}} \\ & +\frac{m+n}{m}\beta_{11}^{(2)}|e_1|^{\frac{n}{m}+\frac{q}{p}}+ae_2^2\} \\ & +[\frac{2mbh}{(m+n)}k_2\left[2(2|e_1|^{\frac{n}{m}+1})^{\frac{2m}{m+n}-1}\right]^2 \\ & +\frac{2mbh}{(m+n)}\frac{1}{k_2}e_2^2+\frac{2m}{(m+n)}(be_2^2)^{\frac{2m}{(m+n)}-1}2be_2h] \\ & +2be_2h+\frac{1}{2}k_1\left|a\beta_{11}^{(2)}\right||e_1|^{2\frac{q}{p}}+\frac{1}{2k_1}\left|a\beta_{11}^{(2)}\right|e_2^2 \\ & -ae_1h+\beta_{21}^{(2)}a|e_1|^{\frac{n}{m}+1}.\end{aligned} \tag{74}$$

The inequality (74) can be recast as

$$\begin{aligned}\dot{V}_{22} \le & -(1-\theta_{22})\{\beta_{11}^{(2)}2(|e_1|^{\frac{n}{m}+1}+be_2^2)^{\frac{2m}{(m+n)}-1}|e_1|^{\frac{n}{m}+\frac{q}{p}} \\ & +\frac{m+n}{m}\beta_{11}^{(2)}|e_1|^{\frac{n}{m}+\frac{q}{p}}+ae_2^2\}\end{aligned} \tag{75}$$

when

$$\begin{aligned}g_{22} = & -\theta_{22}\Bigg\{\beta_{11}^{(2)}2(|e_1|^{\frac{n}{m}+1}+be_2^2)^{\frac{2m}{(m+n)}-1}|e_1|^{\frac{n}{m}+\frac{q}{p}} \\ & +\frac{m+n}{m}\beta_{11}^{(2)}|e_1|^{\frac{n}{m}+\frac{q}{p}}+ae_2^2\Bigg\} \\ & +\Bigg\{\frac{2mbh}{(m+n)}k_2[2(2|e_1|^{\frac{n}{m}+1})^{\frac{2m}{(m+n)}-1}]^2 \\ & +\frac{2mbh}{(m+n)}\frac{1}{k_2}e_2^2+\frac{2m}{(m+n)}(be_2^2)^{\frac{2m}{(m+n)}-1}2be_2h\Bigg\} \\ & +2be_2h+\frac{1}{2}k_1\left|a\beta_{11}^{(2)}\right||e_1|^{2\frac{q}{p}}+\frac{1}{2k_1}\left|a\beta_{11}^{(2)}\right|e_2^2 \\ & -ae_1h+\beta_{21}^{(2)}a|e_1|^{\frac{n}{m}+1}\le 0.\end{aligned} \tag{76}$$

Furthermore, with the constraints $3>2\frac{2m}{(m+n)}$, $\frac{n}{m}+1<2$, $2\frac{q}{p}<2$ and $2(\frac{n}{m}+1)(\frac{2m}{(m+n)}-1) < (\frac{n}{m}+1)(\frac{2m}{(m+n)}-1)+\frac{n}{m}+\frac{q}{p}$ aforementioned, we can conclude that the order of the negative terms is larger than the order of the positive terms in (76).

With the constraints $c_3=\frac{b\beta_{21}^{(3)}}{\delta_1^{1-\alpha_2}}$ and inequality (59), the following results can be obtained from (63):

$$\begin{aligned}\dot{V}_{23} = & -\frac{2m}{(m+n)}2c_3\beta_{11}^{(3)}\frac{e_1^2}{\delta_1^{1-\alpha_1}}(c_3e_1^2+be_2^2)^{\frac{2m}{(m+n)}-1} \\ & -ae_2^2+a\beta_{11}^{(3)}\frac{e_1e_2}{\delta_1^{1-\alpha_1}}-\left(-\frac{a\beta_{21}^{(3)}}{\delta_1^{1-\alpha_2}}+\frac{2c_3\beta_{11}^{(3)}}{\delta_1^{1-\alpha_1}}\right)e_1^2 \\ & +2be_2h\frac{2m}{(m+n)}(c_3e_1^2+be_2^2)^{\frac{2m}{(m+n)}-1}+2be_2h-ae_1h.\end{aligned} \tag{77}$$

We can derive the following inequality according to Young's inequality:

$$\begin{aligned}e_2(c_3e_1^2+be_2^2)^{\frac{2m}{(m+n)}-1} \le & |e_2|(2c_3e_1^2)^{\frac{2m}{(m+n)}-1} \\ & +|e_2|(2be_2^2)^{\frac{2m}{(m+n)}-1}.\end{aligned} \tag{78}$$

Furthermore, we can have

$$\begin{aligned}e_2(c_3e_1^2+be_2^2)^{\frac{2m}{(m+n)}-1} \le & |e_2||e_1|^{\frac{2(m-n)}{m+n}}(2c_3)^{\frac{2m}{(m+n)}-1} \\ & +|e_2|^{\frac{3m-n}{m+n}}(2b)^{\frac{2m}{(m+n)}-1}.\end{aligned} \tag{79}$$

Then the constraint $m<3n$ results in $\frac{1}{2}>\frac{2m}{(m+n)}-1>0$ and $3>\frac{4m}{(m+n)}$. Moreover, with the constraints $0<\theta_{23}<1$ and the inequality (79), we can conclude that the order of the negative terms is larger than the order of the positive terms in

(81). Moreover, the sequel results can be presented as

$$\dot{V}_{23} \leq -(1-\theta_{23})\left[\frac{2m}{(m+n)}2c_3\beta_{11}^{(3)}\frac{e_1^2}{\delta_1^{1-\alpha_1}}(c_3e_1^2+be_2^2)^{\frac{2m}{(m+n)}-1} + ae_2^2-a\beta_{11}^{(3)}\frac{e_1e_2}{\delta_1^{1-\alpha_1}}+\left(-\frac{a\beta_{21}^{(3)}}{\delta_1^{1-\alpha_2}}+\frac{2c_3\beta_{11}^{(3)}}{\delta_1^{1-\alpha_1}}\right)e_1^2\right] \tag{80}$$

when

$$\begin{aligned} g_{23} = & -\theta_{23}\left[\frac{2m}{(m+n)}2c_3\beta_{11}^{(3)}\frac{e_1^2}{\delta_1^{1-\alpha_1}}(c_3e_1^2+be_2^2)^{\frac{2m}{(m+n)}-1}\right. \\ & \left.+ae_2^2-a\beta_{11}^{(3)}\frac{e_1e_2}{\delta_1^{1-\alpha_1}}+\left(-\frac{a\beta_{21}^{(3)}}{\delta_1^{1-\alpha_2}}+\frac{2c_3\beta_{11}^{(3)}}{\delta_1^{1-\alpha_1}}\right)e_1^2\right] \\ & +2be_2h\frac{2m}{(m+n)}(c_3e_1^2+be_2^2)^{\frac{2m}{(m+n)}-1} \\ & +2be_2h-ae_1h\leq 0. \end{aligned} \tag{81}$$

At the switching points, $c_1=|\delta_2|^{\frac{n}{m}-1}$ according to $|\delta_2|^{\frac{n}{m}-1}$ and $c_1=\frac{\beta_{21}^{(1)}}{\beta_{21}^{(3)}}$, and $c_3=|\delta_1|^{\frac{n}{m}-1}$ according to $c_3=\frac{1}{\delta_1^{1-\alpha_2}}$ and $\alpha_2=\frac{n}{m}$, can guarantee $V_{21}=V_{22}$ and $V_{23}=V_{22}$, respectively.

When $V(e)\geq K$ for some $K>0, g_{21}\leq 0, g_{22}\leq 0, g_{23}\leq 0$ and thus $\dot{V}\leq -\tilde{\alpha}(|x|)$ where $\tilde{\alpha}$ is a positive function. The proof of Theorem 2 is finished.

ACKNOWLEDGMENT

The authors would like to thank B.-S. Li for the technical guidance, who is working as a research and development engineer in Shanghai STEP Electric Corporation, Shanghai 201801, China.

REFERENCES

[1] C. Zhang and P. Jiang, "RFID-driven energy-efficient control approach of CNC machine tools using deep belief networks," *IEEE Trans. Autom. Sci. Eng.*, vol. 17, no. 1, pp. 129–141, Jan. 2020.

[2] G. Zhong, Z. Shao, H. Deng, and J. Ren, "Precise position synchronous control for multi-axis servo systems," *IEEE Trans. Ind. Electron.*, vol. 64, no. 5, pp. 3707–3717, May 2017.

[3] M. Hirst, A. McLoughlin, P. Norman, and S. Galloway, "Demonstrating the more electric engine: A step towards the power optimised aircraft," *IET Elect. Power Appl.*, vol. 5, no. 1, pp. 3–13, 2011.

[4] J.-J. Charrier and A. Kulshreshtha, "Electric actuation for flight and engine control; evolution and current trend," in *Proc. 45th Aerosp. Sci. Meeting Exhibit*, 2007, Paper AIAA 2007-1391.

[5] Z. Chen, H. Wang, and Y. Yan, "A doubly salient starter/generator with two-section twisted-rotor structure for potential future aerospace application," *IEEE Trans. Ind. Electron.*, vol. 59, no. 9, pp. 3588–3595, Sep. 2012.

[6] Q. Ze, P. Kou, D. Liang, and Z. Liang, "Fault-tolerant performances of switched reluctance machine and doubly salient permanent magnet machine in starter/generator system," in *Proc. 17th Int. Conf. Elect. Mach. Syst.*, 2014, pp. 3417–3423.

[7] J. Yang, W. Chen, S. Li, L. Guo, and Y. Yan, "Disturbance/uncertainty estimation and attenuation techniques in PMSM drives-a survey," *IEEE Trans. Ind. Electron.*, vol. 64, no. 4, pp. 3273–3285, Apr. 2017.

[8] Y. Wang, Y. Feng, X. Zhang, and J. Liang, "A new reaching law for antidisturbance sliding-mode control of PMSM speed regulation system," *IEEE Trans. Power Electron.*, vol. 35, no. 4, pp. 4117–4126, Apr. 2020.

[9] A. K. Junejo, W. Xu, C. Mu, M. M. Ismail, and Y. Liu, "Adaptive speed control of PMSM drive system based a new sliding-mode reaching law," *IEEE Trans. Power Electron.*, vol. 35, no. 11, pp. 12110–12121, Nov. 2020.

[10] C. Lascu, I. Boldea, and F. Blaabjerg, "Very-low-speed variable-structure control of sensorless induction machine drives without signal injection," *IEEE Trans. Ind. Appl.*, vol. 41, no. 2, pp. 591–598, Mar./Apr. 2005.

[11] C. Lascu, I. Boldea, and F. Blaabjerg, "Variable-structure direct torque control - a class of fast and robust controllers for induction machine drives," *IEEE Trans. Ind. Electron.*, vol. 51, no. 4, pp. 785–792, Aug. 2004.

[12] C. Lascu and G. D. Andreescu, "Sliding-mode observer and improved integrator with DC-offset compensation for flux estimation in sensorless-controlled induction motors," *IEEE Trans. Ind. Electron.*, vol. 53, no. 3, pp. 785–794, Jun. 2006.

[13] I. Boldea *et al.*, "DTFC-SVM motion-sensorless control of a PM-assisted reluctance synchronous machine as starter-alternator for hybrid electric vehicles," *IEEE Trans. Power Electron.*, vol. 21, no. 3, pp. 711–719, May 2006.

[14] C. Lascu, I. Boldea, and F. Blaabjerg, "Comparative study of adaptive and inherently sensorless observers for variable-speed induction-motor drives," *IEEE Trans. Ind. Electron.*, vol. 53, no. 1, pp. 57–65, Feb. 2006.

[15] Y. Jiang, W. Xu, C. Mu, J. Zhu, and R. Dian, "An improved third-order generalized integral flux observer for sensorless drive of PMSMS," *IEEE Trans. Ind. Electron.*, vol. 66, no. 12, pp. 9149–9160, Dec. 2019.

[16] W. Xu, Y. Jiang, C. Mu, and F. Blaabjerg, "Improved nonlinear flux observer-based second-order SOIFO for PMSM sensorless control," *IEEE Trans. Power Electron.*, vol. 34, no. 1, pp. 565–579, Jan. 2019.

[17] W. Xu, M. M. Ali, M. F. Elmorshedy, S. M. Allam, and C. Mu, "One improved sliding mode DTC for linear induction machines based on linear metro," *IEEE Trans. Power Electron.*, vol. 36, no. 4, pp. 4560–4571, Apr. 2021.

[18] W. Xu, A. K. Junejo, Y. Liu, M. G. Hussien, and J. Zhu, "An efficient antidisturbance sliding-mode speed control method for PMSM drive systems," *IEEE Trans. Power Electron.*, vol. 36, no. 6, pp. 6879–6891, Jun. 2021.

[19] Y. Wang, Y. Feng, X. Zhang, J. Liang, and X. Cheng, "New reaching law control for permanent magnet synchronous motor with extended disturbance observer," *IEEE Access*, vol. 7, pp. 186296–186307, 2019.

[20] X. Zhang and Y. He, "Direct voltage-selection based model predictive direct speed control for PMSM drives without weighting factor," *IEEE Trans. Power Electron.*, vol. 34, no. 8, pp. 7838–7851, Aug. 2019.

[21] X. Zhang, L. Sun, K. Zhao, and L. Sun, "Nonlinear speed control for PMSM system using sliding-mode control and disturbance compensation techniques," *IEEE Trans. Power Electron.*, vol. 28, no. 3, pp. 1358–1365, Mar. 2013.

[22] Y. Jiang, W. Xu, C. Mu, and Y. Liu, "Improved deadbeat predictive current control combined sliding mode strategy for PMSM drive system," *IEEE Trans. Veh. Technol.*, vol. 67, no. 1, pp. 251–263, Jan. 2018.

[23] X. Zhang, W. Zhang, C. Xu, Y. Li, Y. Wang, and D. Gao, "Three-dimensional vector based model predictive current control for open-end winding PMSG system with zero-sequence current suppression," *IEEE J. Emerg. Sel. Topics Power Electron.*,vol. 9, no. 1, pp. 242–258, Feb. 2021.

[24] X. Zhang, Y. Li, K. Wang, W. Zhang, and D. Gao, "Model predictive control of the open-winding PMSG system based on three-dimensional reference voltage-vector," *IEEE Trans. Ind. Electron.*, vol. 67, no. 8, pp. 6312–6322, Aug. 2020.

[25] X. Zhang, K. Wang, W. Zhang, Y. Wang, P. Wang and D. Gao, "Dual delay-compensation-based model predictive control for the semi-controlled open-winding PMSM system," *IEEE Access*, vol. 7, pp. 69947–69959, 2019.

[26] X. Zhang, L. Zhang, and Y. Zhang, "Model predictive current control for PMSM drives with parameter robustness improvement," *IEEE Trans. Power Electron.*, vol. 34, no. 2, pp. 1645–1657, Feb. 2019.

[27] L. Qu, W. Qiao, and L. Qu, "An enhanced linear active disturbance rejection rotor position sensorless control for permanent magnet synchronous motors," *IEEE Trans. Power Electron.*, vol. 35, no. 6, pp. 6175–6184, Jun. 2020.

[28] L. Qu, W. Qiao, and L. Qu, "Active-disturbance-rejection-based sliding-mode current control for permanent-magnet synchronous motors," *IEEE Trans. Power Electron.*, vol. 36, no. 1, pp. 751–760, Jan. 2021.

[29] G. Wang, R. Liu, N. Zhao, D. Ding, and D. Xu, "Enhanced linear ADRC strategy for HF pulse voltage signal injection-based sensorless IPMSM drives," *IEEE Trans. Power Electron.*, vol. 34, no. 1, pp. 514–525, Jan. 2019.

[30] Z. Hao *et al.*, "Linear/nonlinear active disturbance rejection switching control for permanent magnet synchronous motors," *IEEE Trans. Power Electron.*, vol. 36, no. 8, pp. 9334–9347, Aug. 2021.

[31] C. Du, Z. Yin, Y. Zhang, J. Liu, X. Sun, and Y. Zhong, "Research on active disturbance rejection control with parameter autotune mechanism for induction motors based on adaptive particle swarm optimization algorithm with dynamic inertia weight," *IEEE Trans. Power Electron.*, vol. 34, no. 3, pp. 2841–2855, Mar. 2019.
[32] Z. Yin, C. Du, J. Liu, X. Sun, and Y. Zhong, "Research on autodisturbance-rejection control of induction motors based on an ant colony optimization algorithm," *IEEE Trans. Ind. Electron.*, vol. 65, no. 4, pp. 3077–3094, Apr. 2018.
[33] J. Han, *Active Disturbance Rejection Control Technique—The Technique for Estimating and Compensating the Uncertainties*. Beijing, China: National Defense Industry Press, 2008.
[34] J. Li, Y. Xia, X. Qi, and Z. Gao, "On the necessity, scheme, and basis of the linear-nonlinear switching in active disturbance rejection control," *IEEE Trans. Ind. Electron.*, vol. 64, no. 2, pp. 1425–1435, Feb. 2017.
[35] Z. L. Zhao and B. Z. Guo, "A nonlinear extended state observer based on fractional power functions," *Automatica*, vol. 81, pp. 286–296, 2017.
[36] S. Vaez-Zadeh, *Control of Permanent Magnet Synchronous Motors*. London, U.K.: Oxford Univ. Press, 2018.
[37] Z. Zhou, C. Xia, Y. Yan, Z. Wang, and T. Shi, "Disturbances attenuation of permanent magnet synchronous motor drives using cascaded predictive-integral-resonant controllers," *IEEE Trans. Power Electron.*, vol. 33, no. 2, pp. 1514–1527, Feb. 2018.
[38] R. Antonello, M. Carraro, and M. Zigliotto, "Maximum-torque-per-ampere operation of anisotropic synchronous permanent-magnet motors based on extremum seeking control," *IEEE Trans. Ind. Electron.*, vol. 61, no. 9, pp. 5086–5093, Sep. 2014.
[39] Z. Gao, "Scaling and bandwidth-parameterization based controller tuning," in *Proc. Amer. Control Conf.*,2003, pp. 4989–4996.
[40] H. Jin *et al.*, "Replacing PI control with first-order linear adrc," in *Proc. IEEE 8th Data Driven Control Learn. Syst. Conf.*, 2019, pp. 1097–1101.
[41] J. Huiyu, S. Jingchao, L. Weiyao, and G. Zhiqiang, "On the characteristics of ADRC: A PID interpretation," *Sci. China Inf. Sci.*, vol. v. 63, no. 10, pp. 258–260, 2020.
[42] B. Guo *et al.*, "A phase-locked loop using ESO-based loop filter for grid-connected converter: Performance analysis," *Control Theory Technol.*, vol. 19, pp. 49–63, 2021. [Online]. Available: https://doi.org/10.1007/s11768-021-00036-0.
[43] M. Safonov, A. Laub, and G. Hartmann, "Feedback properties of multivariable systems: The role and use of the return difference matrix," *IEEE Trans. Autom. Control*, vol. 26, no. 1, pp. 47–65, Feb. 1981.

Ping Lin is currently working toward the Ph.D. degree in navigation guidance and control with the School of Control Science and Engineering, Dalian University of Technology, Dalian, China.

His research interests include nonlinear systems, active disturbance rejection control, and motor control systems.

Zhen Wu received the bachelor's degree in automation from the Hefei University of Technology, Hefei, China, in 2019. He is currently working toward the master's degree in aeronautical and astronautical science and technology with the Dalian University of Technology, Dalian, China.

His main research interests include motor control and active disturbance rejection control.

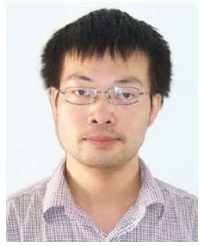

Kun-Zhi Liu received the bachelor's degree in automation from the Harbin University of Science and Technology, Harbin, China, in 2011, and the master's and Ph.D. degrees in control science and engineering from the Dalian University of Technology, Dalian, China, in 2013 and 2017, respectively.

He is currently an Associate Professor with the School of Control Science and Engineering, Dalian University of Technology. His main research interests include hybrid systems, delay systems, and cyber-physical systems.

Xi-Ming Sun (Senior Member, IEEE) received the M.S. degree in applied mathematics from Bohai University, Jinzhou, China, in 2003, and the Ph.D. degree in control theory and control engineering from Northeastern University, Shenyang, China, in 2006.

From 2006 to 2008, he was a Research Fellow with the Faculty of Advanced Technology, University of Glamorgan, Pontypridd, U.K. He then visited the School of Electrical and Electronic Engineering, Melbourne University, Melbourne, VIC, Australia, in 2009, and the Polytechnic Institute of New York University, New York, NY, USA, in 2011. He is currently a Professor of control theory and control engineering with the School of Control Science and Engineering, Dalian University of Technology, Dalian, China. His research interests include aero-engine control, switched delay systems, networked control systems, and nonlinear systems.

Prof. Sun was the recipient of the Most-Cited Article 2006–2010 Award from the journal *Automatica* in 2011. He has been an Associate Editor for the IEEE TRANSACTIONS ON CYBERNETICS since 2014.